Optimisation of Quantum Control Feedback Techniques in an Ytterbium Ion Trap

Supervisor: Dr David Johnson

Ext. Supervisor: A/Prof. Michael J. Biercuk

Quantum Control Laboratory

School of Physics

and

Australian Centre of Field Robotics

Aerospace, Mechanical and Mechatronic Engineering

THE UNIVERSITY OF SYDNEY

Stephen T. Donà

October 2015

For the best mathematician I know,

William McCoy

Acknowledgements

This honours year has been the hardest year of my life, academically and personally. The only way I have been able to achieve what I have this year has been through the support of the people around me.

Mike is my academic idol. His dedication to my work and physics in general is staggering. I want to thank him for the opportunity to do my honours year in the QCL and hope we can continue to work together in the future.

Jarrah showed me how to trap ions. Without his initial help and theoretical foundation I would not have known where to start this year. I want to thank him for being patient with me when I know I could have been a better student.

I would be lost without Sandeep's help in the lab a lot of the time. Knowing he is always there to answer my questions and guide me has given me the academic confidence to achieve this thesis.

I want to thank Virginia for coming to the QCL and helping me in the last part of my Honours year. She has been a tremendous academic help as well as a sympathetic ear when needed.

Harrison, Alistair, Claire, Will, Karsten, Christian, Kehuan and Charlotte have all each helped me this year with either contributions to my physics understanding or simply being a friend. Your all amazing physicists and better people. I consider it an honour to work with everyone I have mentioned so far.

This year has shown me that I have an amazing group of friends who have supported me in my hardest times. I want to thank my brother Anthony and sister

Michelle for accepting my failures and standing by me regardless. Both of you have always been amazing role models to me and I thank you for that.

Finally I would not have survived this year without the unending support from my parents. They have given me everything I have as a man and there are no words that effectively express my gratitude for that.
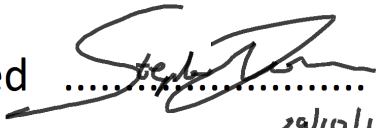
Statement of Contribution

I was the primary experimentalist on the Ytterbium ion trap for which all experimental results presented in this thesis were derived. Unless otherwise stated, all experimental data and analysis was performed by me. Although, previous members of the Quantum Control Labratory did the majority of the trap set-up including the optics and microwave system, I performed some reconstructions after a dismantling early in the year. A major element of my work was based around maintaining, optimising and improving trap elements in order to present the high fidelity experimental results shown in this thesis. Similarly, a lot of the Wavemetrics IGOR code was written before I arrived but there are many elements i rewrote or expanded during my experimentation. All of the MATLAB coefficient optimisation code was written by me.

However, during my honours year I worked alongside many individuals who helped me in my work. Associate Professor Michael Biercuk directed my understanding of Quantum Control and guided my research. He directed me to the appropriate literature and ultimately drove my experimental direction. He also worked with me to draft this thesis. Dr David Johnson provided me the administrative ability to have my engineering honours year in the QCL. Jarrah Sastrawan provided all of the theoretical basis for predictive feedforward and helped me understand the experimental platform early on. Dr Karsten Pyka taught me much about the vacuum system during reconstruction. Dr Sandeep Mavadia has given me everyday experimental guidance and direct help analysising the state estimation data. I worked with Will de Ferranti

to create the native noise reconstruction shown in this thesis. Finally Virgina Frey has help me maintain and run the trap for the final month of this year along with taking some data.

I certify that this thesis, its conception, structure, wording, figures and appearance are all my work where otherwise stated.

Signed ....

29/10/15

"Among other things, you'll find that you're not the first person who was ever confused and frightened and even sickened by human behavior. You're by no means alone on that score, you'll be excited and stimulated to know. Many, many men have been just as troubled morally and spiritually as you are right now. Happily, some of them kept records of their troubles. You'll learn from them - if you want to. Just as someday, if you have something to offer, someone will learn something from you. It's a beautiful reciprocal arrangement. And it isn't education. It's history. It's poetry."

- J.D. Salinger, *The Catcher in the Rye*

Abstract

Before quantum control techniques can be applied to any commercial engineering application, a deep understanding of the precision and accuracy of feedback methods in a quantum setting must be obtained. Similar to most engineered systems, ion control is hampered by a several sources and types of noise ranging from environmental to hardware specific noise which lead to deviations of an oscillator signal from a desired position over time. This thesis attempts to use knowledge about common sources of noise in an ion trapping implementation to assess the effectiveness and precision of feedback methods at suppression and stabilisation of the oscillator deviations. Traditional feedback methods are compared against a novel predictive protocol shown to work theoretically by some members in the quantum control community. Theoretically, the predictive technique uses offline knowledge of the noise frequency spectrum to linearly combine several previous measurements of the noise to perform a more accurate correction than other methods. This thesis explores experimentally the advantages the novel protocol has over traditional feedback methods in precision and accuracy as well as further optimisation techniques using experimental data. Ultimately, the assessment is made as to whether the techniques can be applied practically to enhance the users suppression of error in the ion trap system.

Contents

List of Tables

List of Figures

Chapter 1

Introduction

The development of quantum mechanics, starting in the early 20th century, drastically influenced the direction of scientific research and engineering. Combined with the development of digital computers and the subsequent increase in computational power, new areas of research and design have become feasible for scientists and engineers. The 'first quantum revolution' created many devices used today which are fundamentally reliant on quantum mechanical concepts such as the laser, transistor and semi-conductor [26].

Innovation, development and specifically control of computational and quantum dynamical systems have since been of great interest to scientists and engineers. The latter has been established in mathematics and engineering under the name of control theory. In particular, control theory deals with manipulating a dynamic system employing a feedback pathway that consists of taking a reference as to what the system is doing and then correcting the system's overall state to a desired orientation in real time. In modern times, it is possible to solve multivariable and non-linear control problems [46, 50, 15]. One specific example of a non-linear control problem is quantum control in which the system's dynamics are governed by the laws of quantum mechanics. Quantum control has manifested itself as an independent aspect of control

theory, as classical control theory is unable to deal with characteristics peculiar to quantum system. However, classical theory layed most of the theoretical foundation.

The study of quantum feedback control has practical and fundamental value for science and engineering. Not only have experiments performed by Khaneja et al. and Nielsen et al. [43, 29] shown that quantum control can contribute to stabilising nuclear magnetic resonance (NMR) and computational complexity respectively, but blooming from quantum control are furthering ideas and innovations in other areas such as frequency standards and quantum simulation. More recently, Yacoby et al. [45] have used Hamiltonian estimation feedback to control quantum coherence in an attempt to establish scalable quantum information technology. These areas of research deal with the control of one or more frequencies with the use of measurement based feedback.

A popular example is the problem of a passive frequency standard, which is producing a highly accurate and stable frequency reference. Worldwide standards such as Caesium fountains and hydrogen masers can only achieve this level of accuracy through control algorithms designed to suppress frequency errors and instabilities within the system. As these standards are inherently quantum systems, it is thought that the further development of quantum control techniques would be beneficial to these implementations [42].

This work makes experimental contributions to the understanding and development to quantum control feedback algorithms in the context of frequency standards. The experimental platform is a linear Paul ion trap in which a quantum system is realised by cooled and isolated Ytterbium ions. This thesis is structured as follows: Chapter 1 outlines the theoretical concept of qubit control and give the underlying motivation of the experimental work. Chapter 2 describes the principle of ion trapping and the specific details of the experimental setup. Chapter 3 outlines the methodology employed to perform reliable quantum measurements in noisy environments. Chapter 4 presents the concept of combining quantum measurements to produce more accurate

state estimation than previously used methods and analyses experimental results. Chapter 5 concludes and discusses the possibility of future work.

1.1   Qubits and the Bloch Sphere

The concept of coherently manipulating a qubit, the quantum analogue to the classical bit, is a fundamental concept in quantum control. Theoretically, a qubit can be based on any coupled two state quantum mechanical system in nature. Unlike the classical bit which can only represent two possible states, typically represented by 1 and 0, a qubit can be any superposition of the two. The state of the qubit, $|\Psi\rangle$ can be expressed by the linear combination shown in equation 1.1 where α and β are complex probabilities of finding a $|0\rangle$ and $|1\rangle$ state respectively.

$$|\Psi\rangle = \alpha\,|0\rangle + \beta\,|1\rangle \tag{1.1}$$

As this concerns quantum probabilities, the state must be normalised, *i.e.* $|\alpha|^2 + |\beta|^2 = 1$ and either α or β can be chosen to be real. The canonical parametrisation can be written as [18]

$$|\Psi\rangle = cos\left(\frac{\theta}{2}\right)|0\rangle + e^{i\phi}sin\left(\frac{\theta}{2}\right)|1\rangle \tag{1.2}$$

in terms of two real numbers θ and ϕ with natural ranges $0 < \theta < \pi$ and $0 < \phi < 2\pi$. As these are analogous to polar angles on a 3-dimensional sphere, a geometrical representation of the pure state space of the qubit has been used by the community and is called a Bloch sphere.

A Bloch sphere is a unit sphere centered around a coordinate origin. A Bloch vector extends from the origin to a point on the surface of the Bloch sphere. Conventionally, the $|0\rangle$ state is represented by the North Pole of the sphere and the $|1\rangle$ state, the South Pole. States on the equator correspond to the superposition states of equal weighting but different phase, represented by ϕ. Given any state on
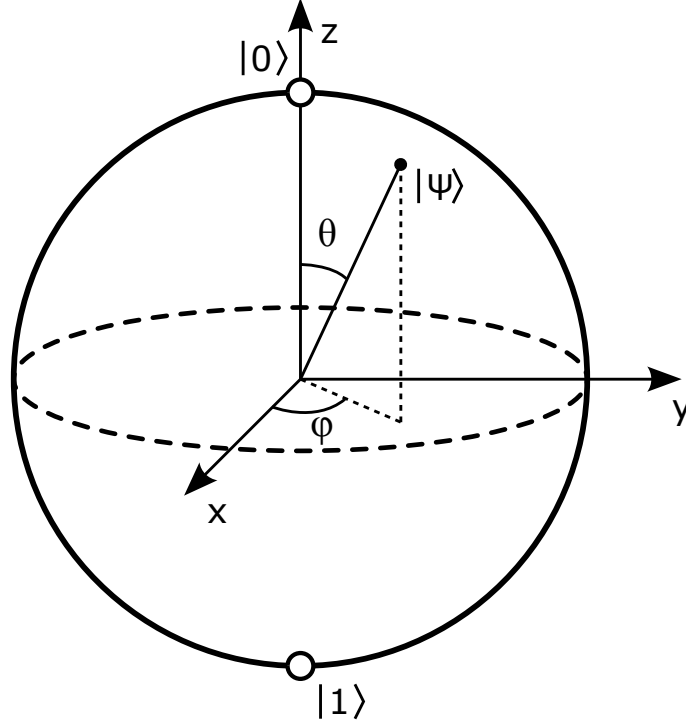
Figure 1.1: A Bloch sphere represents a superposition state as a vector from origin to the surface of a sphere. Angles θ and ϕ are the polar and azimuthal angles of the vector on the sphere.

the sphere, the diametrically opposite point will represent the negative dipole and hence an orthogonal state.

1.1.1 Rabi Oscillations

In terms of control, it is important to derive a result to perform manipulations on the Bloch vector. This can be achieved through the interaction of the qubit system with a classical field $(\boldsymbol{E}(t))$. A two level quantum state will have a population density matrix as follows

$$\rho(t) = \begin{pmatrix} \rho_{11} & \rho_{12} \\ \rho_{21} & \rho_{22} \end{pmatrix} \tag{1.3}$$

4

where the on diagonal entries are population densities of the $|0\rangle$ and $|1\rangle$ states respectively and the off diagonal entries are called coherences and represent the response of the system at the driving frequency. The time evolution of this matrix follows from the Schrödinger equation with the Hamiltonian $H = H_A + H_1 = H_A - \boldsymbol{\mu}(t) \cdot \boldsymbol{E}(t)$):

$$\frac{\partial \rho(t)}{\partial t} = \frac{1}{i\hbar}[H, \rho(t)] \tag{1.4}$$

where $\boldsymbol{\mu}(t)$ is the charge density. This can be expressed as four general equations of motion where ω_0 is the atomic resonance frequency

$$
\begin{aligned}
\dot{\rho}_{11} &= \frac{1}{i\hbar}[\langle 1| H_1 |2\rangle \rho_{12} - c^2] \\
\dot{\rho}_{22} &= -\frac{1}{i\hbar}[\langle 1| H_1 |2\rangle \rho_{21} - c^2] \\
\dot{\rho}_{12} &= \frac{1}{i\hbar}[-\hbar\omega_0\rho_{12} + \langle 1| H_1 |2\rangle (\rho_{22} - \rho_{11})] \\
\dot{\rho}_{21} &= \frac{1}{i\hbar}[\hbar\omega_0\rho_{21} + \langle 1| H_1 |2\rangle (\rho_{11} - \rho_{22})]
\end{aligned}
\tag{1.5}
$$

These equations of motion can be translated to change in position of the Bloch sphere vector components. These equations are called the *Bloch Equations* and are expressed as

$$
\begin{aligned}
\dot{r}_1 &= \frac{2}{\hbar} \text{Im}[\langle 1| H_1 |2\rangle]r_3 - \omega_0 r_2 \\
\dot{r}_2 &= -\frac{2}{\hbar} \text{Re}[\langle 1| H_1 |2\rangle]r_3 - \omega_0 r_1 \\
\dot{r}_3 &= -\frac{2}{\hbar} \text{Im}[\langle 1| H_1 |2\rangle]r_1 + \frac{2}{\hbar} \text{Re}[\langle 1| H_1 |2\rangle]r_2
\end{aligned}
\tag{1.6}
$$

If we consider the rotating frame of reference, these equations of motion simplify to

$$
\begin{aligned}
\dot{r}_1' &= \delta r_2' \\
\dot{r}_2' &= \Omega r_3' - \delta r_1' \\
\dot{r}_3' &= -\Omega r_2'
\end{aligned}
\tag{1.7}
$$

where Ω is the atomic transition frequency and δ is the detuning of the radiation from atomic resonance [14]. If we combine these three equations in one vector representation we arrive at one of the most important physical results in terms of qubit manipulation;

$$\dot{\boldsymbol{r}}' = \boldsymbol{r}' \times (\Omega\hat{\boldsymbol{e}}_{\boldsymbol{x}} + \delta\hat{\boldsymbol{e}}_{\boldsymbol{z}}) = \boldsymbol{r}' \times \boldsymbol{W} \tag{1.8}$$

This equation shows that it is possible to evolve the system state by driving it with with a resonant field. The evolution follows rotation along the W vector. These driven rotations are the fundamental process used to manipulate the qubit state. Figure 1.2 shows the mechanics of a rotation visually.
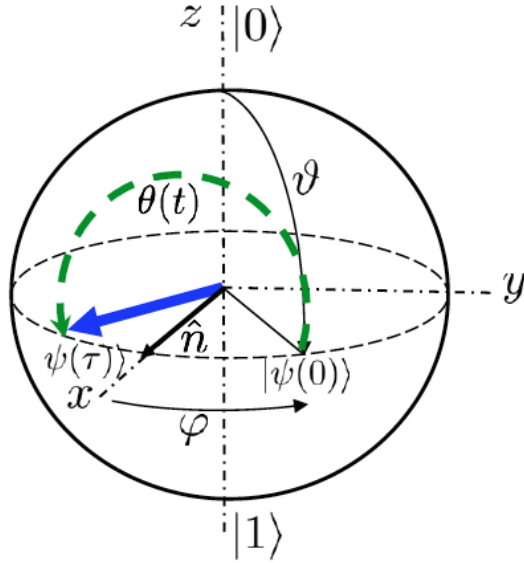
Figure 1.2: Example of driven rotation in the Bloch Sphere. The amplitude of the driving field determines the rate of rotation. Figure from [16].

In the case of $\delta = 0$ in equation 1.8, W $= \Omega\hat{\boldsymbol{e}}_{\boldsymbol{x}}$ and the evolution of the Bloch vector follows a great circle from $|0\rangle$ to $|1\rangle$ and back again [40]. This frequency of rotation is equal to Ω and labeled the 'Rabi frequency'. The time the external electromagnetic field is needed to be exposed to the qubit to produce a half revolution (π revolution) is calculated as it is extremely important for the following experiments and this time is called the π time. The π time is calculated by exposing to the qubit

to an electromagnetic field so that it oscillates and measurements of the quantum state are taken at regular intervals. These oscillations are called Rabi oscillations or Rabi flopping. Once several rabi oscillations have been performed on the qubit, it is possible to accurately measure the π time from the measurements. The time of electromagnetic exposure and detuning frequency of the radiation (δ) are the primary manipulations used to control the Bloch vector and hence the superposition state of the qubit.

1.2   The Qubit Control Problem and Decoherence

As mentioned previously, the quintessential qubit control problem contains manipulating a qubit superposition state by applied rotations. In order to differentiate the qubit control problem from a classical control problem the specific difficulties encountered in the quantum regime will be briefly discussed.

An inherent difficulty with any quantum system is the quantum state will be effected by noise due to interactions with the environment. The effect of this noise on the system is to induce 'decoherence' into the system which means that over time the state will become a random superposition and all quantum information will be lost[48]. Decoherence may be thought of in two general classes: Energy relaxation and transverse dephasing [4]. Energy relaxation affects the longitudinal angle (θ) which in turn effects the probability amplitudes of the qubit. The characteristic time over which a system 'relaxes' is known as T_1 as it has historic roots in the NMR field [52]. The process of transverse dephasing involves the randomisation of the phase difference between the basis states. Such phase randomisation leads to a decay in coherence over a time (T_ϕ). In total, these two decoherence processes lead to a finite useful lifetime of any quantum setup. This lifetime is known as T_2 and is calculated by $T_2^{-1} = T_\phi^{-1} + (2T_1)^{-1}$. From the perspective of an experimentalist or engineer, qubit coherence times are most often dominated by transverse dephasing processes.

If we consider this dephasing in our state population density matrix we arrive at this formalism;

$$\rho(t) = \begin{pmatrix} \rho_{11} & \rho_{12}e^{-2i\int_0^t y(t)dt} \\ \rho_{21}e^{2i\int_0^t y(t)dt} & \rho_{22} \end{pmatrix} \quad (1.9)$$

where y(t) is the random dephasing fields imparted by the environment. This shows the off diagonal coherence decay to zero with an ensemble average and mathematically defines the decoherence process [9].

Rather than attempt to solve the 'decoherence' problem, the work in this thesis is performed in such a way that it can be considered insignificant.

1.3 Frequency Standards

The stable frequency reference or standard is a key laboratory requirement and can be sourced from several devices and methods [23]. The commercial metric for measuring the performance of a frequency standard is Allan variance. Quartz oscillators, Caesium fountains and hydrogen atomic references all vary in performance depending on the observation period (τ). In general, quartz crystals provide greater improvement in the short term ($\tau < 10$ s) however at longer time scales ($\tau > 100$ s) greater stability is associated with the atomic frequency standards. Caesium is specifically stabile as the frequency errors are bounded by the accuracy limits and properties of the setup such as vacuum pressure and laser power rather than the measurement interval. This means that highly accurate frequency measurements can be made at very long time spans with equal accuracy as short ones, however the currently observed stability (Allan Variance $= 10^{-13}$) will likely not be bettered without experimental improvements seen in [2, 10].

A passive frequency standard consists of a slave oscillator driven by an atomic resonator response (possibly from a Caesium fountain or Hydrogen Maser). This slave oscillator then gives a frequency input to a frequency synthesizer to produce the

uniform field to drive the qubit rotations; completing the feedback loop. The stabilsed reference is then 'picked off' from the slave oscillator. Obviously, any instability in the master atomic reference will be carried over to the slave oscillator so it is important that the atomic resonator chosen can produce long term frequency stability in respect to the intrinsic noise on the slave oscillator.

1.3.1 Stabilising a Local Oscillator with Atomic Frequency Reference Control
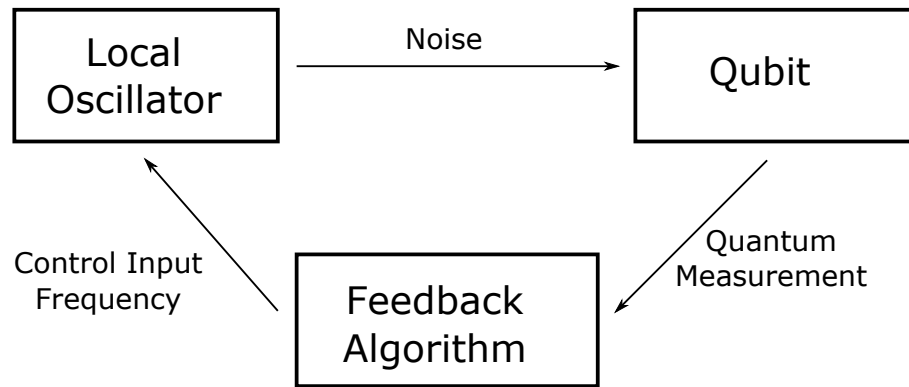
Figure 1.3: The simplified linear control problem is one where a local oscillator produces noise in a considerable 'noiseless' qubit. Through measurements and manipulations of the quantum state, it is possible we can correct the local oscillator to be tuned to the qubit frequency

The focus of this work will be stabilising and estimating the state of a local vector signal generator (VSG) given the qubit frequency as a passive reference. If we consider the source of noise not from the qubit itself but rather a local oscillator and that the frequency perturbations in the qubit are essentially non-existent, the problem only becomes one of measurement based feedback on the local oscillator rather than performing feedback on qubit coherence. In order to stabilise the LO, a closed feedback pathway will be implemented as shown in Figure 1.3. Measurements of the quantum system will be taken using sequences of driven rotations in the Bloch sphere. If the experimental regime is only considered in times much shorter than the

time taken for the qubit to develop decoherence, this can be ignored. However, it should be noted that the local oscillator stability highlights a lot of similiar aspects to the decoherence problem. The major point of difference and hence the motivation for simplifying the problem is the dephasing feedback considered in the LO feedback simplifies the problem to linear control and allows us to use measurement based feedback control discussed in chapter 3.

Chapter 2

Relevant Ion Trapping Concepts
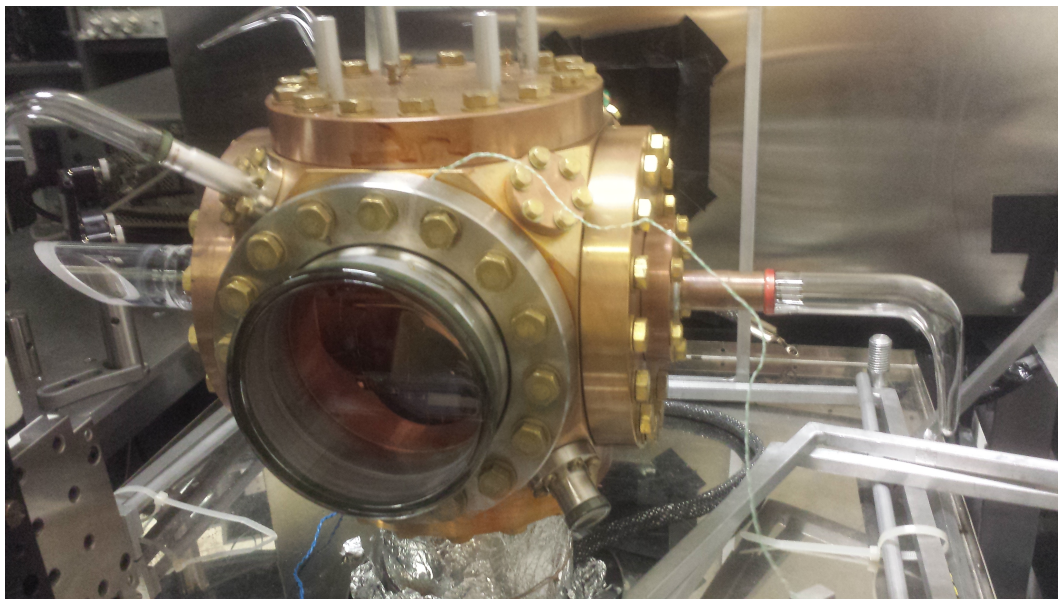
Figure 2.1: Experimental ion trap platform

An extremely powerful apparatus to test these feedback protocols is an ion trap [41]. In the isolated environment of an ion trap, it is possible to create a clean stable reference frequency with the use of an internal electronic transition frequency of a trapped ion. Ion traps also provide advantages in the way of extremely high accuracy control over the electronic degrees of freedom, extremely long ion lifetimes and internal state coherence times [33]. Although the current SI definition of a second is based

on Caesium, ion based experiments have recently shown higher accuracy frequency measurements due to environmental advantages [38]. The development of ion trapping knowledge and expertise throughout the scientific community is an equally important goal as ion trapping is still in its infancy and showing promise in many other scientific and engineering applications including mass spectrometry and electron accelerators [6].

2.1 Ion Trap Design

The ion trap is the main piece of apparatus used to perform the experiments presented in this thesis. The primary objective of the ion trap is to contain a number of atomic ions in one space using a combination of electric or magnetic fields, kept under ultra high vacuum (UHV). At first it seems impossible to bound any set of ions as Earnshaws theorem states "a charged particle cannot be held in a stable equilibrium by electrostatic forces alone"[17]. This is confirmed by Maxwells equation $\nabla.E = 0$, [17] which ultimately describes that any electric field orientation will always allow the ions to be free in some direction. It was shown by the 1989 Nobel Laureates Hans Georg Dehmelt and Wolfgang Paul that ion trapping could be performed using a magnetic field or a dynamic electric field respectively [34, 8]. Named after its inventor, the Paul trap uses an rf signal to create the dynamic electric field required to trap ions and is the type of trap that is used in these experiments.

2.1.1 Paul Trap Potentials and Geometry

Fisk's summary [12] explains how an arrangement of fields can produce confinement for an electric potential. If we consider the one dimensional point ion of mass, m and charge q being effected by a oscillating electric field of frequency Ω and amplitude function, $E_0(x)$, then the position of the particle given standard zero inital conditions is derived as
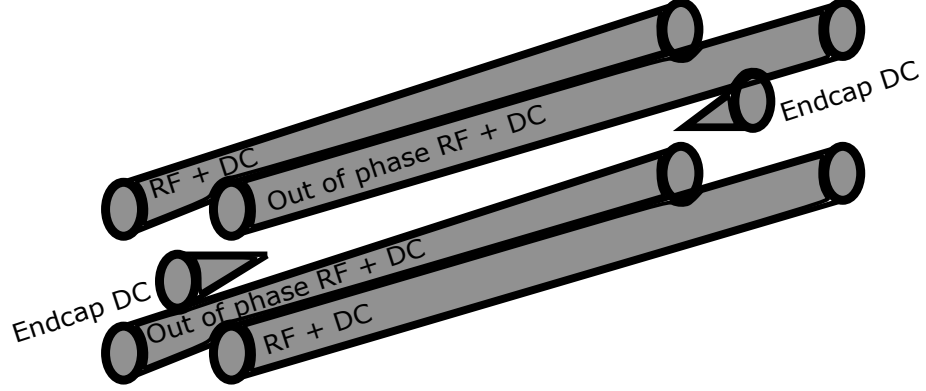
(a) 4 rod linear Paul trap
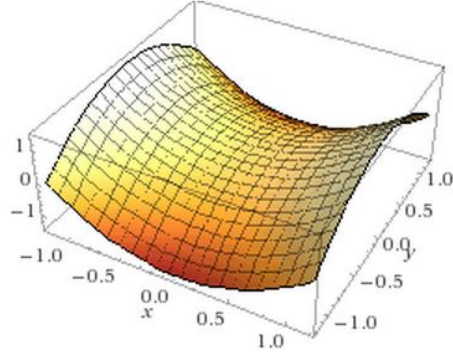
(b) The electric field potential of DC voltages on rods
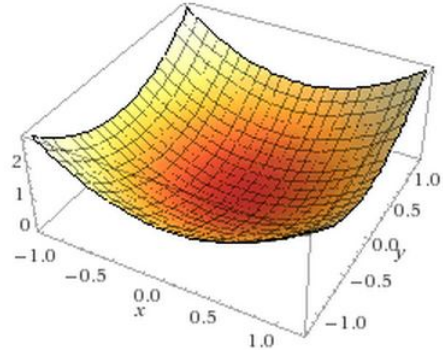
(c) The time averaged electric field from DC and RF

Figure 2.2: The saddle shaped potential shown in (b) is created when only DC voltages are applied to the four rod trap design shown in (a). When a RF voltage is applied to either diagonally opposite rods or as in phase and out of phase pairs as shown, the potential will effectively rotate resulting in the potential shown in (c).

$$x(t) = \frac{-qE_0(x)}{m\Omega^2}cos(\Omega t) \tag{2.1}$$

For large ω the deviation of from its average position is very small and the psuedopotential approximation can be made. Any electric field E(x) that satisfies Maxwell's equations and $\nabla^2 E > 0$ can trap charged particles [55]. This is usually achieved with a combination static DC voltages and oscillating AC voltages resulting in a quadrapole potential at the centre of the trap.

It has been shown by Prestage et al. [35] that physical geometry required to produce this quadrapole is four parallel metal RF carrying rod electrodes with

two sharpened DC carrying 'end-cap' electrodes shown in Figure 2.2a. It should be noted that this produces a *linear* Paul trap which gives the advantages of a larger psuedopotential minimum resulting in more ions trapped then the conventional hyperbolic counterpart as well as greater magnitudes in tuning distance by the DC end caps. It is shown that if a DC voltage is applied to all rods in this geometry that the voltage potential produced is a hyperbolic saddle shape given by equation 2.2 [33].

$$V_{hyp} = \frac{V_0}{2}cos(\Omega t)\Big(1 + \frac{x^2 - y^2}{R^2}\Big) \tag{2.2}$$

To achieve an infinite paraboloid, an RF voltage must be added to effectively achieve a continuous swapping of the x-y orientation of the potential. This can be achieved by applying an RF to diagonally opposite rods, however experimentally this is done in addition to applying an out of phase by one half-wavelength RF voltage to the other diagonally opposite rods. As the main value that effects the electric potential is the difference between the adjacent rod voltages, the out of phase RF additional voltage effectively doubles the resultant electric field. It has been derived that the equation of motion of a charged particle in one axis due to this potential and oscillation is given by the equation

$$\ddot{x}(t) = \frac{e^2V_0^2}{2m^2\Omega^2R^4}x \tag{2.3}$$

The solution to the differential equation 2.3 gives our simple harmonic oscillator and RF frequency, $\omega_x = \frac{eV_0}{\sqrt{2}m\Omega R^2}$. As this same reasoning could be applied in the y direction, it is shown that charged ions will not be released from the ion trap.

In the linear Paul trap used experimentally, the general operational values for the RF frequency was 425 kHz and the amplitude of 150 V_{pp} Differences in the DC voltage applied to each rod is controlled and monitored for the purpose of shimming, the process whereby spontaneous asymmetries in the trapping potential are compensated for with a DC bias perpendicular to the oscillating field. These asymmetries occur

spontaneously due to unwanted charge build up on the conducting elements inside the vacuum chamber and on the trap mount so shimming must be done regularly to ensure the ions are placed centrally in the trap.

2.2 Ytterbium Energy Level Structure
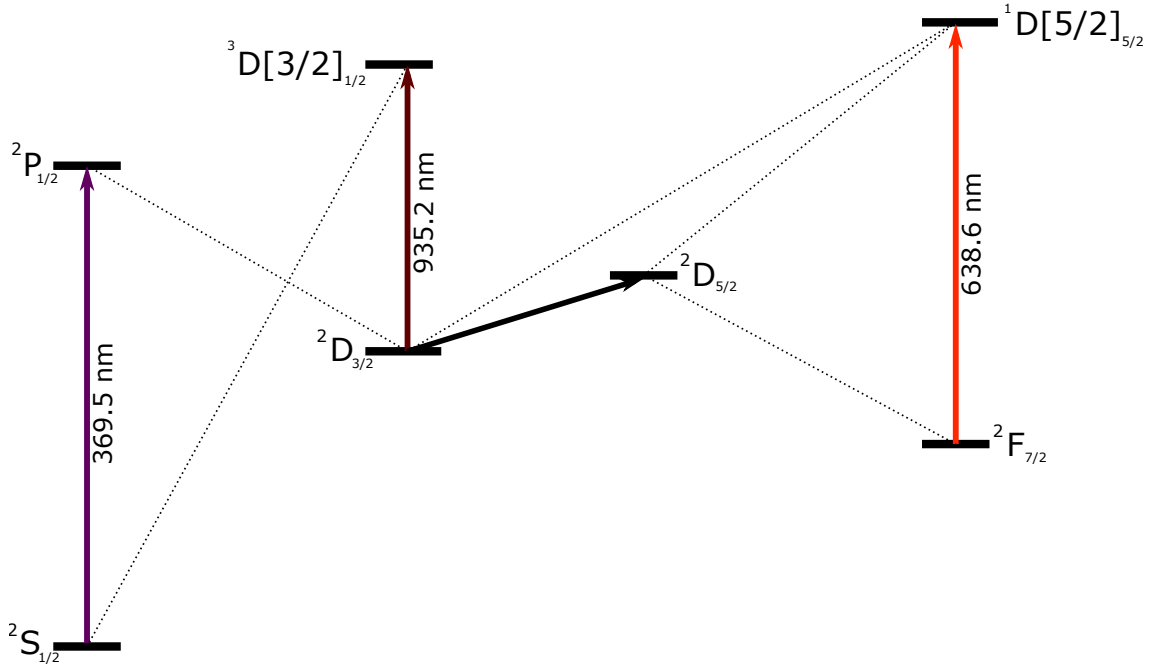
Figure 2.3: Gross Energy level structure for all Ytterbium ions. The solid lines depict transition that can be driven by lasers where the dotted lines depict likely decay routes. Ytterbium is ionised into the $^2S_{1/2}$ state which can be driven into the $^2P_{1/2}$ state using UV laser. However from the P state, decay into unwanted D and F states are possible so secondary repump lasers are necessary to energise the ions into a higher states that will decay back into the S-P transition.

Although almost any element can be ionised and trapped, Ytterbium-171 isotope is used as it gives an excellent experimental qubit environment. More specifically, the relevant energy transition levels are found in a range that can be accessed by commercial lasers and optical products such as fibers and optical filters. Moreover, the large fine structure of Yb$^+$ makes it amenable to fast manipulaitons with broadband

laser pulses. All Ytterbium ions produce the gross energy level structure in Figure 2.3.

The Ytterbium ion energy structure is based around three optical transitions. The most relevant transition is the 369.5nm S to P state transition as this will be used for cooling and detection. However it should be seen that from the $^2P_{1/2}$ state there is a 0.5% chance of decaying to a $^2D_{3/2}$ intermediate state rather than re-emitting UV radiation and falling the the ground state. This $^2D_{3/2}$ state has a relatively long lifetime (approximately 53 ms) and adds a second complication as it can decay to the very stable $^2F_{7/2}$ with the lifetime of 5.4 years.
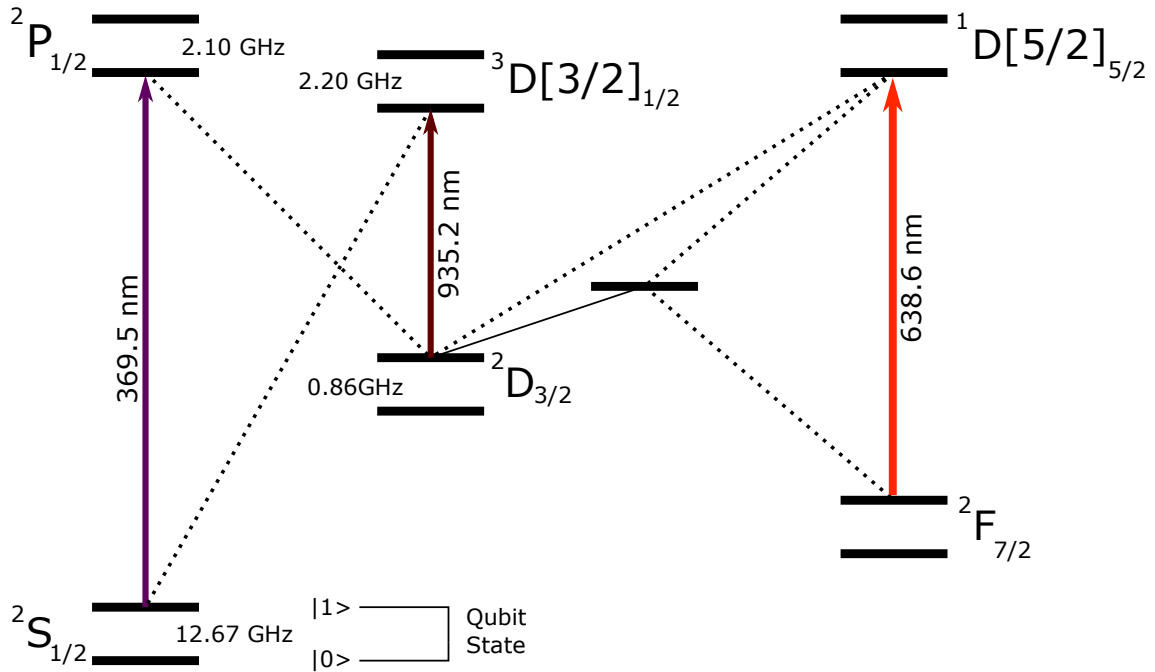
Figure 2.4: Energy structure of Ytterbium-171 showing the hyperfine splitting of each state and the frequency 'gap' between each split state. Notice the top and bottom of the 369nm transition is 2.10 GHz and 12.67GHz respectively

Ytterbium-171 is targeted as its odd number of protons and neutrons produces a half nuclear spin generating a hyperfine doublet on each of its energy levels and this splitting is what creates the desired qubit environment [32]. The hyperfine splitting of these state produce a 2.105 GHz difference in the $^2P_{1/2}$ state and 12.643 Ghz difference

in the lower $^2S_{1/2}$ state. In total this produces a 14.7 GHz difference between the largest energy level and lowest.

The qubit state is defined by the magnetic hyperfine dipole transition that exists in the $^2S_{1/2}$ ground state. This transition is known as a clock transition as its first order is insensitive to magnetic fields, protecting it and making it specifically useful as a frequency standard [33, 13]. In order to drive the qubit uniformly over the whole cloud, the magnetic dipole must be spacial controlled by a static uniform magnetic field across the cloud.

2.3 Optical Transitions

There are a number of transitions within the Ytterbium ion energy level structure that can be driven using lasers of appropriate energy. Most of the key optical absorptions require laser's in the ultraviolet, optical or infrared range.

2.3.1 Two-stage Photoionisation

The first and most important optical drivien transition is the act of ionisation to initially to fill the trap. During the first stage of trapping, an oven is required to heat the Ytterbium to a level at which it creates a thermal cloud of atoms [19]. Although some traps use purified sources of Ytterbium isotopes, the ionisation sample can contain all naturally occurring isotopes of ytterbium in their relative abundances.

Isotope	Abundance
^{168}Yb+	0.13%
^{170}Yb+	3.04%
^{171}Yb+	**14.28%**
^{172}Yb+	21.83%
^{173}Yb+	16.13%
^{174}Yb+	31.83%
^{176}Yb+	12.76%

Table 2.1: Stable Yb+ isotopes and their relative abundances. Values from [24]

In order to completely ionise the neutral Ytterbium thermal gas, two state transitions must be driven by UV lasers. As seen in Figure 2.5, Ytterbium initially in the $^1S_0$ state can then be excited to a $^1P_1$ state and finally into the ion continuum. The first transition has a resonant frequency of 398.9 nm and second transition requires a photon with the energy of at least a 394.1 nm wavelength.[19] To perform this second transition, a laser of 369.5nm is commonly used as that laser is also used in Doppler laser cooling of the ions (see section 2.3.2).
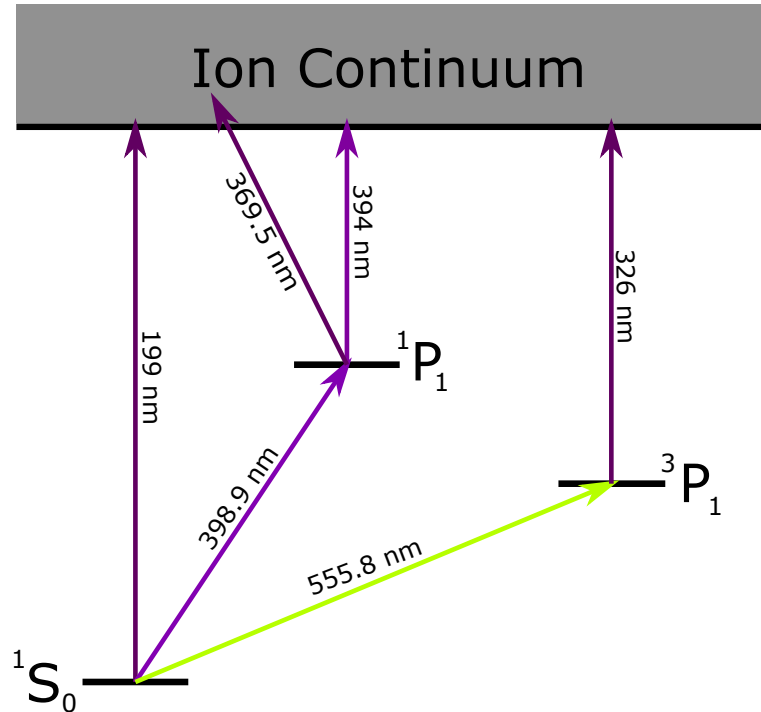
Figure 2.5: Relevant Energy pathways to the ionised Ytterbium continuum. The middle 398.8nm and 369.5nm path is the described path which all the experiments in this thesis use. However, the other possible ways to ionise neutral ytterbium should be noted.

All Isotopes are ionised by this method, however it is important to consider the Doppler shift seen by the atom in the thermal cloud as this will be used to specifically select the Ytterbium-171 isotope [36]. Due to this Doppler shift each isotope will required a slightly different frequency for the first stage of ionisation and from experimental optimisation, the Ytterbium-171 isotope frequency can be found.

2.3.2   Laser Cooling

Once an electric potential parabolic well has been established and loaded with ions by processes described in section 2.1.1 and 2.2, Wineland et al. and Neuhauser et al. have both independently shown that the cloud can be laser cooled to a level where quantum information experiments can be run [56, 28]. The goal of laser cooling is to reduce the ion energy to a level applicable to the experiment. This is achieved by a process of absorption and emission in such conditions that the net energy change for the ions is a loss. In our experiment, this is achieved through Doppler cooling. If incoming photons have frequency slightly below that of the excitation transition frequency or resonance, the atoms moving towards the light source will be more likely to absorb these photons due to the Doppler Effect [25]. Each absorption imparts a momentum kick of $\bar{h}k$ into the ion in the opposite direction of motion. The release of that energy will always be a random spontaneous scatter event with no favoured direction and hence we can assume that the momentum kick from the photon release averages to zero in large clouds over many iterations of this process. This means that as absorption causes an average lose in momentum and emission does not, it can be seen that the net effect is an overall damping for atomic force and reduction of kinetic energy. It should be noted that due to the fact that the ions do reemit the photons that the ion cloud can only be cooled to a certain Doppler limit.

Doppler cooling of Yb is usually achieved using the 369.5 nm laser detuned slightly below that of the $^2S_{1/2}$ to $^2P_{1/2}$ transition discussed in section 2.2. There are methods to cool below the Doppler limit and many QIT experiments require those limits [44, 20]. In the experiments described in this thesis, it is acceptable to work close to the Doppler limit and optimise the cooling by equally splitting the beam into one straight beam and one offset beam at an angle that are recombined in the centre of the trap [41].

As described in section 2.2 Ytterbium-171 ions cause hyperfine splitting of quantum states and will require frequency sidebands to be able to cool from

all substrates as well. This frequency sidebands are added using Electro-Optic Modulators (EOM). The device uses an RF signal to add sideband frequencies on to a main source laser in integer multiples both above and below the carrier frequency. To account of the hyperfine splitting at both the S and P state a 14.75 GHz sideband must be added which is achieved experimentally by the second order sideband of a 7.325 GHz EOM.

2.3.3   State Initialisation

Using EOMs to achieve the goal of adding sideband frequencies to our cooling lasers is particularly powerful as it allows us to easily detect and control states. For example, if the 7 GHz EOM is turned off but the 369.5nm laser is allowed to continue through the trap, the ion will only have the supplied photon energy to make the transition from the high S state to the lower P state. This will not cool the ions but rather form a closed subspace that prevents change in the relative populations of ion states, resulting in an unambiguous qubit state measurement. This is the conditions that are required and used for state detection. Using a combination of the cooling laser and the EOMs we can create any combination or superposition of energy states inside the ^{171}Yb ion energy state structure. The ^{171}Yb 171Yb ion is our qubit state will be labeled 0 and 1 as shown in the figure. See section 2 for details on how this qubit is controlled and manipulated for experimental results.

2.3.4   Depopulation of Possible Other States

As mentioned previously, it is possible that that the $^2P_{1/2}$ state can decay into a $^2D_{3/2}$ state. It is very important for most ion trap experiments that this state is recycled back into the 369nm transition. This is performed by a 935.2 nm repump laser which is also ran through a fiber 3.067 GHz EOM. The final laser used is a visible 638.6nm laser that is used similarly to the 935nm laser to recycle ions out of an $^2F_{7/2}$ state that it has possibly fallen into from the $^2D_{3/2}$ state. This second level decay into an

unwanted state happens at such a slow rate that this laser does not need a EO to attach sideband frequencies to it but it rather just moves back and forth between the two required frequencies every 20 or so seconds.

2.4   Experimental Realisation

In order to perform high fidelity experiments, the appropriate apparatus must be constructed and maintained.

2.4.1   Laser Setup

In order to achieve accurately driven transitions described in section 2.3, a series of lasers that fit a set of criteria must be used. The criteria is as follows;

- narrow linewidth (< 5 MHz)

- long term frequency stability or the functionally to be effectively stabilised.

- precisely tunable sidebands

Each of these criteria can be achieved by commercial external cavity diode lasers (ECDL) from MOGLabs which are stabilised by a wavemeter. Sidebands are added to appropriate beams using EOMs and controlled using TTL- trigged switches from an external PC. In this implementation it is possible to apply and remove the sidebands or beam path in time frames less than a millisecond.

Electro-Optic Modulators

Each EOM modulates a monochromatic laser beam with an input electrical signal. This is usually achieved with Pockel cells, an electro-optic crystal through which laser light can propagate but will modulate phase delay if a voltage is applied across it. The Pockel cell thus acts as a voltage controlled waveplate. The principle behind the

phase delay is the *electro-optic effect* which states that it is possible to modify the refractive index of a crystal with an electric field [11]. As the refractive index changes in parts of the crystalline structure, the input laser light will be delayed in phase. The polarisation of the input laser must be aligned with the optical axis as it will be effective if it is not.

2.4.2 Laser Stabilisation

The frequencies of all the lasers mentioned are continuously and cyclically measured using a wavelength detection meter, commonly referred to as a 'wavemeter'. In practical implementation, a High-Finesse/Angstrom WSU U-10 was used which monitored up to eight frequencies at once using optical switches. Every wavemeter requires a stable frequency reference that it is calibrated to. An absolute Helium-Neon laser was chosen as it is extremely stable over long time periods and allows up to 10 MHz absolute frequency accuracy [21]. The IR and visible beams can be sent into the wavemeter using a commercially standard optical switch that is TTL triggered by the wavemeter but due to manufacturing limitations the UV lasers must use alternative solutions. A custom-built free space switch and a flip-flop circuit controlling two AOMs are used to TTL-trigger into the wavemeter.

The wavemeter can then be used to lock the lasers to desired set frequency points using in-built measurement based feedback in real time. The measurements of frequency are transmitted to a PC which uses software analogous to a PID controller that sends a signal to the wavemeter to output a set of control voltages. These control voltages are applied to each lasers piezoelectric control crystal which stabilises the laser output frequency. The wavemeter works predominantly in switching mode which applies corrections in a cycle to all lasers, completing one set in approximately half a second which results in less than kilohertz deviations which is acceptable for the experiments undertaken in this thesis. It is possible that more sophisticated
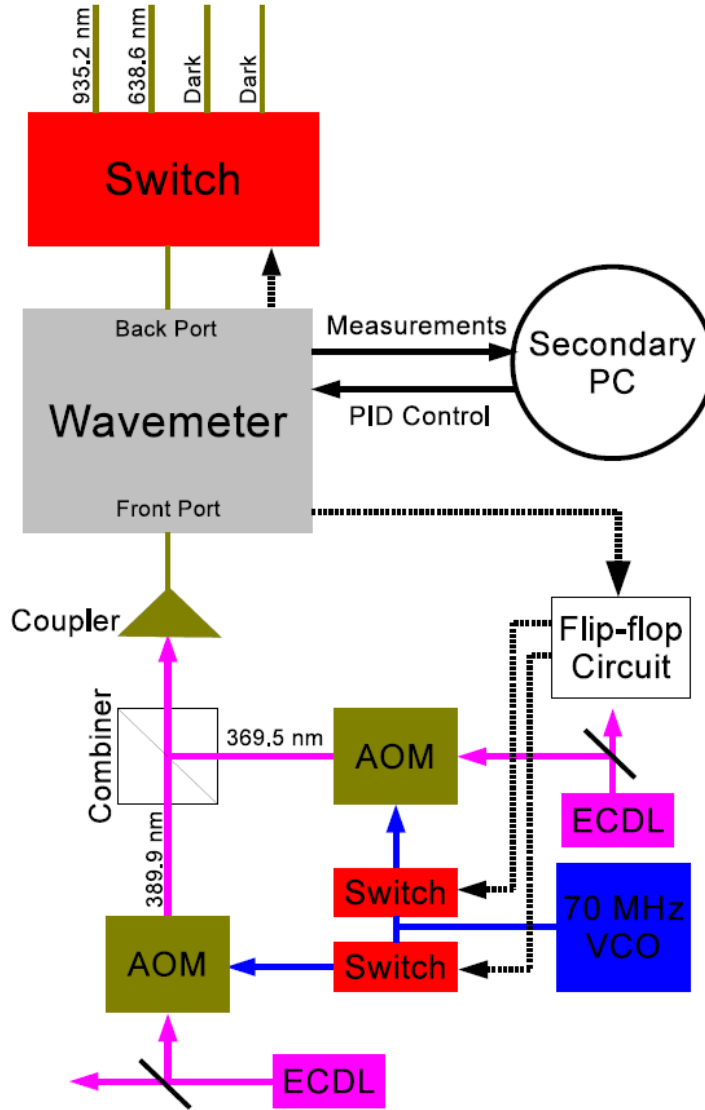
Figure 2.6: In this experimental configuration, the wavemeter accepts the UV laser light from the front port and the rest of the lasers from the back switch. The wavemeter then sends the measurement outcome for each channel to the PC via USB and trigger a flip-flop circuit via TTL. The cycling of the four laser inputs is done by both the switch, cycling the IR and visible laser with two unused inputs. Simultaneously the two flip-flop circuit cycles through 8 chances with the two UV lasers on the second and third channel. The AOM's act is 'shutters' rapidly switching on and off to create and destroy the relevant beam lines. The external PC controls the laser frequency using PID control values. Figure from [41]

stabilisation at higher bandwidth is possible with Pound-Drever-Hall locking or the use of a Fabry-Perot optical cavity with current feedback [21, 22].

2.4.3 Helmholtz Coils
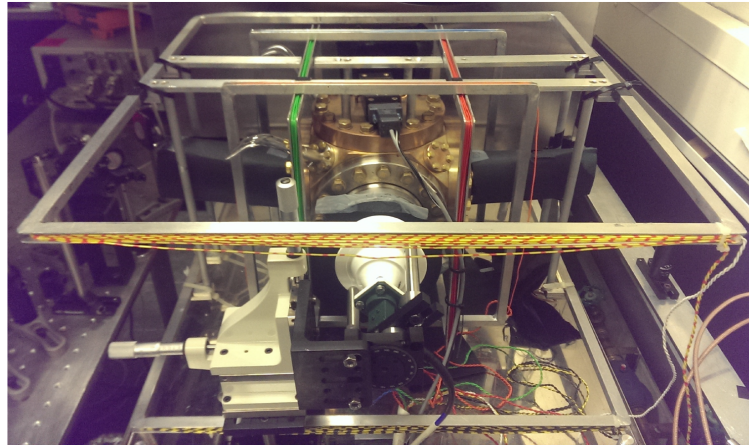
(a) Front View
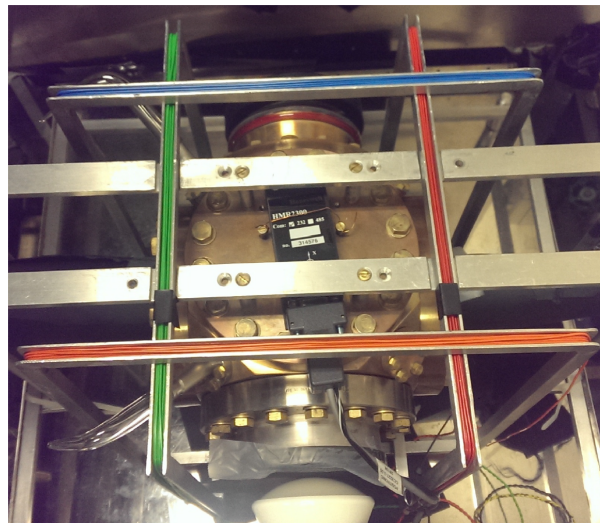
(b) Top View

Figure 2.7: Side and top views of the three sets of Helmholtz coils around the vacuum chamber which allow for modifications of the magnetic field. The white microwave horn is visible in the centre of the top view (a) and the black magnetometer is visable in the center of the front view (b)

As mentioned in section 2.2 a magnetic field is required to produce the hyperfine doublet. Experimentally, this magnetic field is provided by three pairs of Helmholtz coils which have an applied DC voltage. With the use of magnetometer, the Earth's nature magnetic field is monitored and the appropriate voltages are applied to the

coils to cancel all components leaving the appropriate magnetic field. Each coil pair will produce a homogeneous field across the ions which ultimately add to the product B field in the $\hat{y}$ direction. The application of this magnetic field does create a slight Zeeman splitting of the $|1\rangle$ into a triplet however the trap and vacuum chamber is magnetically insulated from the ambient magnetic fields by a Ni-Co shield. This allows the linearly polarised optical and microwave electromagnetic waves to preferentially target all three states in the case of the optical lasers (cooling radiation) and a single state in the case of the microwaves (driving radiation).

2.4.4   Ultra-High Vacuum
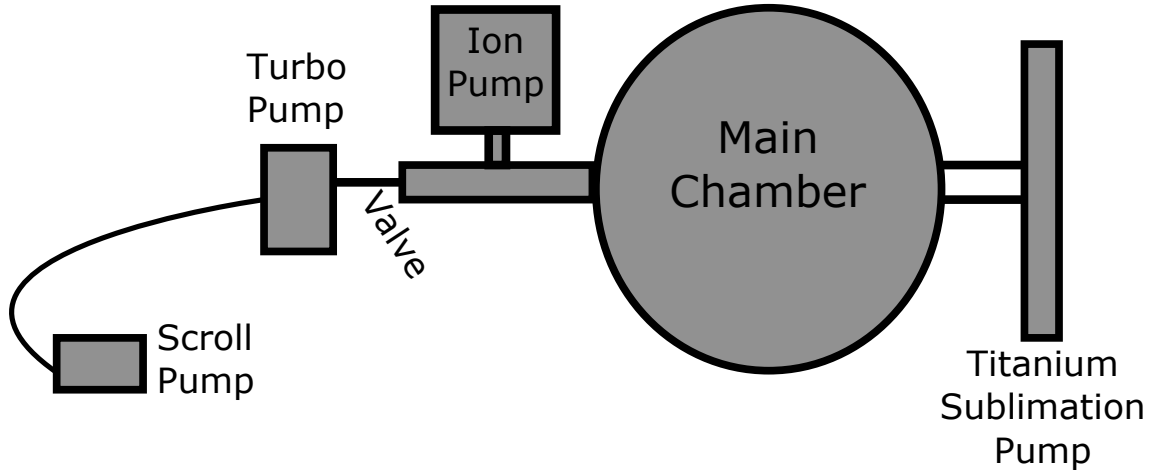
Figure 2.8: Diagram of experimental vacuum setup. before the valve is closed and the turbo and scroll pump are removed.

After the trap has been constructed and the lasers set up to combine in the centre of the four rod trap, the atomic ions will only be trapped in ultra-high vacuum (UHV) environment to ensure long trapped ion lifetime. Ideally, the trap chamber is reduced to a pressure of 10^{-11} to minimise the average ion collision to the order of a few every hour [33]. To achieve this extremely low pressure, all vacuum chamber components need to be sealed using ConFlat all-metal pieces with stainless steel knives edges and copper gaskets. Any organic matter inside the trap will disrupt the UHV chamber.

As well as this, it is essential that the each component separately and the trap fully assembled is baked at approximately 250 degrees as this establishes a chromium oxide layer on the surface of the steel that reduces outgassing of hydrogen [31]. To maintain the UHV a series of pumps are used in succession which include a roughing scroll pump, a turbo pump, an ion pump and a titanium sublimation pump. The scroll pump is to assist the turbo pump which is only used primarily to get the pressure low enough such that the ion pump is effective (around 10^{-6} Torr). After this is achieved, the turbo and scroll pump can be turned off via a value connection to the main chamber and detached entirely.

2.4.5   Detection System

Figure 2.9: Camera screenshot of approximately 400 Ytterbium ions trapped in linear paul trap

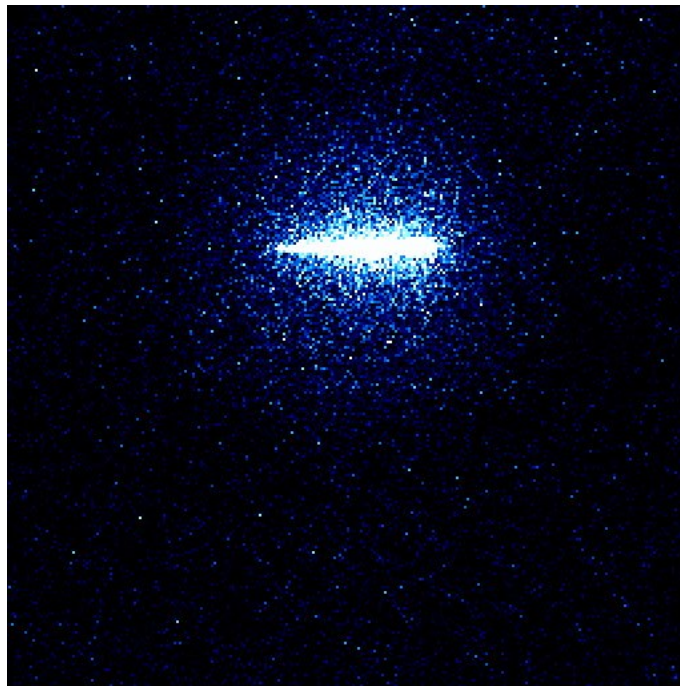The key pieces of apparatus included in the detection system is a camera, a photomultiplier tube (PMT). The camera and PMT are not simultaneously recording the ion cloud as there is only one glass viewing plate on the trap chamber. Instead,

each device is attached to a set of precision translation stages (ThorLabs NRT100E) which are also controlled by the PC. The translation stages are programed to move between two set of coordinates which are regularly optimised to maximise detection. The image of ions inside the trap is focused using a telescopic system including two lens; a 100mm diameter Knight optical lens with a 160mm focal length followed by an 80mm diameter lens with a 100mm. This combination of lens reduces the image size and by ratio 0.625 so that it will be the optimal size for the camera and PMT aperture.

When the ion cloud is sufficiently cooled, the ion cloud fluoresces when interacting with the ultraviolet 369 nm laser. If an ultraviolet filter is used in conjunction with a CCD video camera (Andor Solis iXon Ultra High Speed) it is possible to clearly view and determine the $^2S_{1/2} \rightarrow^2 P_{1/2}$ resonant frequency as well as the estimate size of the cloud. This is done during the initial loading and cooling of the ions to effectively build an appropriate cloud for experimentation. As we are dealing with a large ensemble of ions, the cloud's fluorescence intensity will be directly proportional to the probability of find a $|1\rangle$ state and hence can be considered a good determination of the z-axis projection of the superposition state on the Bloch sphere. A PMT combined with a gate photon counter (Stanford Research Systems SR400) can be used to transmit accurate cloud intensity measurements to a PC running Wavemetric's IGOR program using RS-232 serial connections. Being performed this way, it is easy to analytically use those counts in IGOR computationally and the time period of photon counting can be precisely controlled for very accurate photon count measurements. The counting period changed depending on the parameters of the experimentation, however this value is generally 1ms. The accuracy of the photon counter is increased with a UV filter and aperture to cut out all light frequencies ± 10 nm of the cloud florescence frequency.

Projective measurement of Quantum State

An aspect of quantum measurement which was made famous by Schrödinger's cat is that measurement of the qubit destroys any superposition state that previously existed [3]. It is possible to still effectively measure the superposition state or probabilities of finding each state by measuring an ensemble of atoms all at once. Even though it is possible to construct and use an ion trap in such a way that only traps one or two atoms, experimentally for this thesis, approximately between one hundred and one thousand atoms are used in an attempt to gain statistically significant information about the qubit superpositional state and bypass the wavefunction collapse dilemma.

2.4.6 Microwave Setup

It is relevant to mention the microwaves discussed in this section must satisfy a series of very specific criteria. These criteria are as follows; [41]

1. Frequency of 12.6Ghz (Ytterbium Qubit Frequency)

2. High power

3. Spatial homogeneity over the ion cloud

4. Extremely high accuracy of frequency

5. Extremely high frequency power and polarisation stability

This means that the microwaves must be produced by a very sophisticated signal generator (Agilent vector signal generator E8267D) which must be frequency stabilised by a Caesium fountain source and cleaned using a Wenzel Crystal. This clean signal is then passed directly into a microwave horn at which is focused into the trap centre using a lens. It is important to note that the microwaves must have a linear polarisation aligned parallel to the qubit dipole axis. There are many ways to apply microwaves to the trapped ion cloud including applying microwaves to the

trap rods or a microwave antennae [47]. The benefit of using a microwave horn in this set up is that the microwaves can be more easily controlled in terms of power and direction.
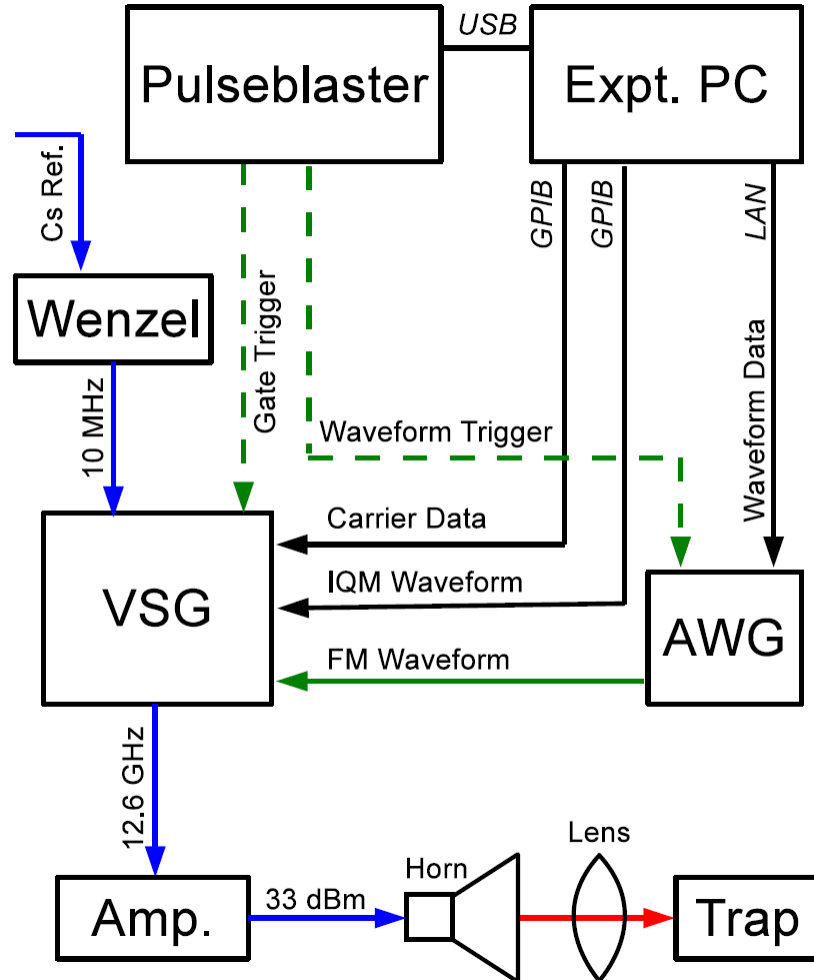
Figure 2.10: The VSG is controlled by gate triggers from a pulseblaser and set up via GPIB connections with the experimental PC. The VSG is frequency modulated by an arbitrary waveform generator which is also controlled by PC. This signal could then be amplified and fed into the microwave horn to apply to the ions. Figure from [41].

Chapter 3

Qubit Stabilisation using Measurement Feedback

In any quantum laboratory environment, qubit state decoherence and dephasing is a constant and severe problem as any experiment setup will require a stable local oscillator as a reference. The problem lends itself well to control engineering as he noise can be considered as random perturbations of a classic field and no quantum mechanical treatment of the feedback is required [51]. Any local oscillator (LO) component will unintentionally accumulate phase noise inherent to the design of the system [1]. If we consider how this phase noise will affect the frequency we can see that it will attribute a time dependent frequency variation by the following equations;

$$f \propto \frac{d}{dt}(\text{phase}) \tag{3.1}$$

if phase $= \phi_0 + \Delta\phi$ then

$$f = f_0 + \dot{\phi}(t)$$

If these variations are allowed to develop over time, it is possible to accumulate noise is a way to make all quantum measurements meaningless. Any timing

oscillator used experimentally will have intrinsic phase noise instabilities from the underlying hardware so will always require control methods to suppress this phase noise accumulation [42]. Measurement based feedback can be used to compensate for this given an absolute reference is available to transfer the stability to [38]. As it is considered that the qubit frequency is entirely isolated from the environment, it can be used as the absolute reference to stabilise any experimental laboratory local oscillator reference.

3.1   Ramsey Experiments

Ramsey experiments or Ramsey interferometry is a method that manipulates the atomic state of a qubit to extremely accurately measure atomic states [7]. The Ramsey experiment involved a series of microwave applications at specific time to achieve a measurement result and is the primary way used experimentally to measure the qubit state [37]. The method of a Ramsey experiment is as follows;

1. Use laser EOMs to force all ions to $|0\rangle$ state (dark ground state).

2. Apply microwaves for a half pi time. This will allow the qubit state to rotate by pi/2 from the dark state towards to the equator of the Bloch sphere.

3. Wait a certain amount of time (Ramsey time). This free evolution time is important as during the Ramsey time the qubit frequency will slightly detune itself from the Microwave vector generator due to a series of sources of noise. This detuning can be represented as a separation in the polar angle of the Bloch sphere. Both the vector generator and qubit Bloch vectors are still on the sphere's equator as the slow .

4. Apply a second half pi time. This microwave will rotate both vectors another half pi rotation towards the $|1\rangle$ bright state vector in the Bloch sphere. However both will be rotate in the plane that contains the vector signal generator (VSG)

Bloch vector. The VSG will always end up in a perfect $|1\rangle$ state but if the qubit
has detuned from the VSG then it will not get rotated down entirely and end up
in some superposition state rather than a pure $|1\rangle$ bright state. The difference
the qubit is from the from the $|1\rangle$ bright state is dependent on the amount of
detuning that occurred during step 3, the Ramsey time [53].

The power of Ramsey experiments is that they can be run repeatedly and can
accurately show the degree and rate of detuning in the local oscillator with respect
to the qubit frequency.
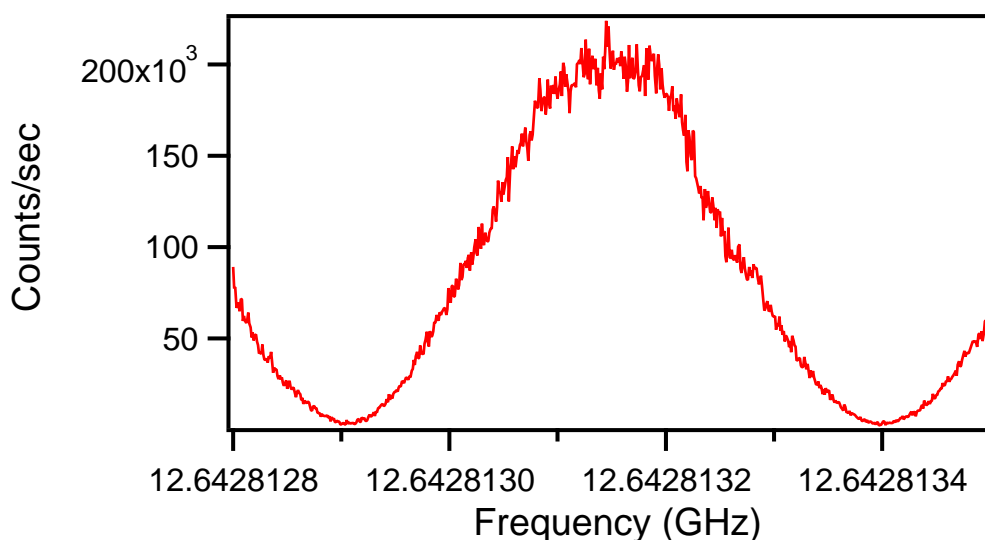
Figure 3.1: Experimental measured frequency envelope or 'Ramsey Fringe'. A
Ramsey experiment was taken over a series of oscillator frequencies for a set Ramsey
time (t_r). This plot shows the clear maximum centered around the qubit frequency
i.e. the Ramsey experiment that was exactly in tune with the qubit frequency will
produce maximum brightness.

Ramsey spectroscopy can also be used to locate the centre (qubit) frequency
with a series of ramsey experiments taken over a frequency scan. If the detuning is
large in either the positive or negative direction, the second $\frac{\pi}{2}$ pulse will rotate away
from the bright state and less fluorescence will be seen. However if the frequency is
aligned to the qubit frequency, we will see maxmum brightness as seen in the centre
of figure 3.1. After a frequency scan as been performed it possible to calculate the

centre frequency by fitting a sinusoidal function and deriving the maxmised brightness frequency position.

3.2 Frequency Offset Measurement using Square Wave Frequency Modulation

In the context of the feedback control experiments, a single Ramsey experiment can only achieve a measurement of the magnitude of detuning but not the sign. Performing Ramsey experiments in close vicinity to the resonant qubit frequency produces a symmetric Ramsey fringe and therefor equal brightness whether detuning occurs in the positive or negative directions. This is problematic if we wish to use this method for frequency measurement feedback as deviation direction is essential knowledge. To overcome this, we perform two Ramsey experiments, one with the VSG frequency detuned slightly over the qubit frequency and one slightly below. The ideal detuning distance is a calculated as $\pm\frac{\Gamma}{2}$ where Γ is the full-width half maximum (FWHM) of the fringe.
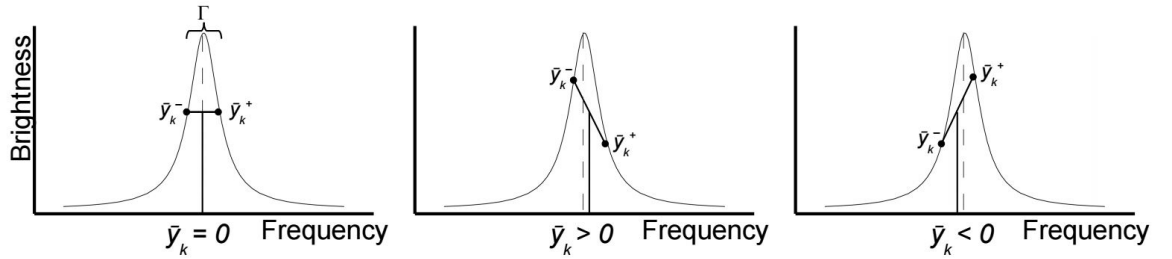
Figure 3.2: If the frequency has shift, the resultant measurements of the ramsey fringe will also be effected. The sign of the difference between the two measurements can be used to determine the sign of the frequency shift. Figure from [41].

To perform this frequency shift, the experiment relies on rectangular wave frequency modulation of the carrier microwaves. Experimentally, this is achieved through an external arbitrary waveform generator which produces a rectangular wave

which is sent into the microwave vector signal generator's external FM input port, The frequency (f) and amplitude (A) of the waveform generated externally is calculated by the PC using the following equations which we always result in measuring at the correct FWHM point;

$$f = (t_r + t_d)^{-1} = (t_{cycle})^{-1} \tag{3.2}$$

$$A = \frac{1}{2t_r} \tag{3.3}$$

Once measurements have been taken either side of the fringe, it is possible to make a gradient calculation based on the logic described in figure 3.2 if it is assumed the values fall on a sinusoidal fringe. If $\Delta p = y^+ - y^-$ then the calculation for the frequency offset would be;

$$\delta = \frac{1000 \arcsin \Delta p}{2\pi t_r} \tag{3.4}$$

This offset can be added the qubit frequency to find the absolute frequency using this method.

3.3   Characterising Noise

In physics, noise is any random fluctuation of an electrical or mechanical signal and can occur in many different types with several causes. The type of noise of interest is the inherent noise on the local oscillator which is assumed to dominate the noise of the qubit. The character of noise is defined by its power spectral density (PSD). A power spectral density is a distribution of powers or amplitudes over a series of frequencies. The function which governs the power over frequency is the determining factor in the flavour of noise [30]. The Wiener-Khinchin theorem can used to derive filter transfer functions that capture the spectral effect of particular interrogation schemes. The

simplest experimentally-useful variance metric is called the true variance [39, 54] and is defined as following;

$$
\begin{aligned}
\sigma^2(k) &= E[\bar{y}_k^2] \\
&= E\left[\left(\frac{1}{t_r}\int_{t_{e,k}}^{t_{s,k}} y(t)g(t - t_{s,k})^2 dt\right)\right]
\end{aligned}
\tag{3.5}
$$

where y(t) is the noise function, g(t) is a time reversable sensitivity function and $t_{s,k}$ and $t_{e,k}$ are the start and end time respectively of the measurement, M_k. Applying the Wiener-Khinchin result to the PSD and Fourier transforming the sensitivity function gives;

$$
\sigma^2(k) = \frac{1}{2\pi}\int_0^\infty S_y(\omega)|G_k(\omega)|^2 d\omega
\tag{3.6}
$$

where $|G_k(\omega)|^2$ is the transfer function for the kth sample and $S_y(\omega)$ is the power spectral density function. Some simple examples of $S_y(\omega)$ are as follows;

- $F(\omega) \propto \omega^0$. This is white noise and is a combination of all frequencies in equal amounts which allows the higher frequency components to dominate. Almost all electrical devices will have some intrinsic white noise level as a product of its electrical conduction. Due to is universality, white noise construction and optimisation will be targeted to be reduced by frequency standard feedback algorithms.

- $F(\omega) \propto \omega^{-1}$. This is usually referred to as flicker noise or pink noise and is very similar to white noise which more low frequency dominating components. This character of noise will be analysed the most heavily by frequency standard experiments as it is extremely common in experimental setups. Experiments usually have a component of white noise as described above but also a series of lower frequency noise sources, e.g. temperature fluctuations, air current movements, etc which combine to create a total flicker noise character in the local oscillator.

- $F(\omega) \propto \omega^{-2}$. This is random walk noise is almost entirely dominated by low frequency components. This will be tested by frequency standard experiment but not as a primary target as it rare that an experiment only has random walk noise as its noise error source.

- Along with any of these characters of noise, it is possible to add spurs (unusually high power amplitudes) at specifc frequencies or multiples of frequencies. This is also a condition that is important to investigate as it is commonplace that spurs occur in electrical devices and quantum systems.

Power Spectral Densities of Common Noise Types

It was important to choose noise types and engineered noise parameters such as strength and cutoff frequencies in such a way to focus the efforts of analysing feedback techniques for this project. It is well understood that thermal noise (white noise) is unavoidable [27] in all electronic devices as it is generated by random thermal motion of charge carriers inside the conductor regardless of applied voltage. With this in mind, it became a priority to understand what gains could be made with a flat noise power spectral density. It will also become a priority to measure the intrinsic noise in the system to see what possibly could be corrected for in the future.

3.4 Engineering Noise

In order to gain a higher degree of control in experiment and show that the techniques presented in this thesis have the ability to succeed in the presence of any arbitrary noise power spectral density, it is important to engineer any noise spectral density required, specifically focusing on the noise types observed in real laboratory conditions. To create this deliberate error, we can use a control PC to degrade the microwave signal frequency in any required time domain realisation of a noise PSD. This is done by taking an average of the noise trace between the start and end times

of the measurement $[t_{s,k}, t_{e,k}]$ and applying that frequency to the VSG at the time of measurement. This results in the qubit experiencing the effective average noise over the time of measurement. It is important that the engineered noise is scaled to always dominate the effect of the intrinsic phase and amplitude noise in the microwaves, so that the intended engineered noise ultimately reflects the desired noise type.

The standard design for engineered noise PSDs is to model one or more of the power law types described in section 3.3 between two start (ω_{start}) and stop (ω_{stop}) frequencies. At these boundaries, two roll-off functions ($R_{low}(\omega)$ and $R_{high}(\omega)$) are defined in equation 3.7 to ensure the function is continouse over the whole domain.

$$S(\omega) = \begin{cases} R_{low}(\omega) & \text{for } \omega < \omega_{start} \\ \sum_{\alpha=-2}^{2} A_\alpha \omega^\alpha & \text{for } \omega_{start} < \omega < \omega_{stop} \\ R_{high}(\omega) & \text{for } \omega > \omega_{stop} \end{cases} \tag{3.7}$$

Common 'roll-off' functions used in these experiments include a 'white ceiling' ($R(\omega) = \text{constant}$) or a hard cutoff ($R(\omega) = 0$) although its possible it include almost any function desirable to replicate real noise scenarios. To effectively use the PSD in these experiments, the fourier transform must to taken to obtain the time-domain realisations of the frequency and phase errors [49]. The phase noise and frequency noise time-domain waveforms as a discrete truncated inverse Fourier transform are;

$$y_\omega(t) = A_\omega \sum_{j=1}^{j_c} F_\omega(j) sin(\omega_j t + \chi_j) \tag{3.8}$$

$$y_\psi(t) = A_\psi \sum_{k=1}^{k_c} F_\psi(j) cos(\omega_k t + \chi_k) \tag{3.9}$$

The values of $A_{\omega,\psi}$ are the overall noise scaling factors, the subscript c denote the maximum frequency or phase comb index, and $\chi_{\omega,\psi}$ is a randomly seeded additional phase. It can be seen that the Fourier transform is a sum of sine wave at specific comb frequencies ($\omega_j = j\omega_0$) together with random phases. As Fourier transforms are

difficult to be calculated for discrete functions, experimentally simply adding sines is an effective implementation.

3.4.1 Engineered Noise Measurement Parameters

After a time domain noise trace has been effectively created, it must be measured and applied to the qubit for experimentation. This raises some important control parameters in terms of noise measurement, application and feedback design. To mirror the qubit measurement technique of the continuous noise trace must be applied in bins of discrete time lengths (T_m^k). As the noise is continuous and will be freely evolving during these measurement bin times, the control design of the engineered noise takes the average over the bin time and applies it to the qubit. As the measurement bin time is increased, the system will become less effective at measuring high frequency components and this must be considered during experimentation. As well as this, the inherent noise will be measured as larger as the longer time between Ramsey experiments can result in a larger magnitude frequency difference.
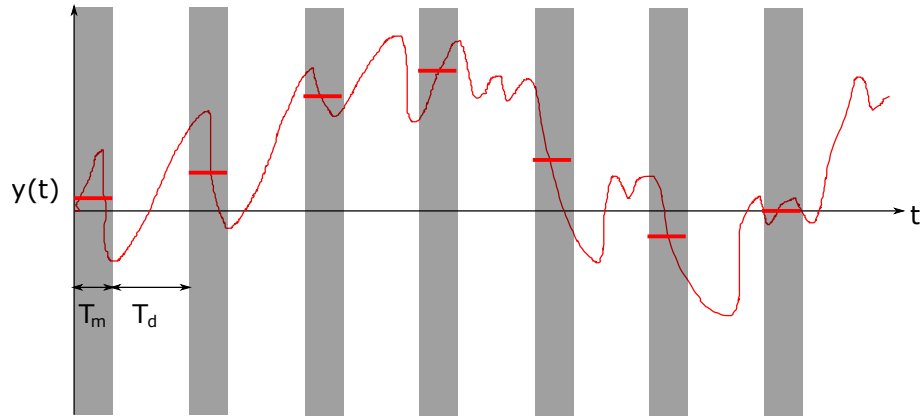
Figure 3.3: Over the time of measurement (T_m^k), the noise is average to a discrete value which can be applied to the VSG and hence the qubit system. In this diagram we have several measurements taking place with some dead time (T_d^k) although in reality the deadtime can be minimised. Any higher frequency than $\frac{1}{2t_{cycle}}$ will effectively be 'invisible' to the noise sampling as a it is faster than the Nyquist frequency [5].

It is possible to inject dead time between measurements as this ultimately shows robustness in the feedback methods. It is important to show that any feedback algorithm can not only stabilise a local oscillator but also accurate predict the noise state at some given time in the future (t_c). It is important that the experimental regime tested shows that as the deadtime increases, the correlation between successive measurements decreases. This would mean that the noise is fast changing relative to the cycle time. The percentage of measurement time to the entire cycle time (measurement and deadtime) is referred to as the duty cycle of the experiment.

3.4.2 Engineered Noise Strength and PSD Parameters

Once it was designed that an arbitrary noise wave form of any PSD could be engineered, the noise parameters were optimised to engineer the noise types of interest. As described in section 3.4, it would be impossible using our noise engineering methodology to create 'pure' white noise with infinitely man frequency components. To combat this, we experimented with the frequency cutoff points in order to create what is known as 'pseudowhite noise' (white noise with a cutoff at some point). Specifically the upper cutoff frequency became extremely important in defining the 'quasistatic limit', which is the limit of fast changing noise in relation to the dead time.

Although these values changed over the course of the year with different experimentation, commonly used values for pseudowhite noise were $\omega_{start} = 0.001$ Hz, $\omega_{spacing} = 0.001$ Hz and $\omega_{stop} = 0.5$ Hz for a 20 ms measurement time. These values ensured that the noise was fast changing relative to the deadtime but not the measurement time in 1% duty cycle experiments. It is extremely important from here to choose noise strength (multiplication factor A) which meant that the engineered noise always dominated over the intrinsic noise in the system. If this was not the case, no clear results could be found about the effectiveness of feedback techniques

on the certain experimentally tested noise regimes. In order to effectively determine this strength, information about the native or intrinsic noise is required.

3.5 Measurement Experiments

During the beginning of the analysis, a series of measurement experiments were run to highlight the effectiveness and fidelity of the experimental setup. The experiments undertaken was a measurement of the intrinsic or native noise in the system and to measure a series of engineering noise traces. The results of these experiements were as follows;
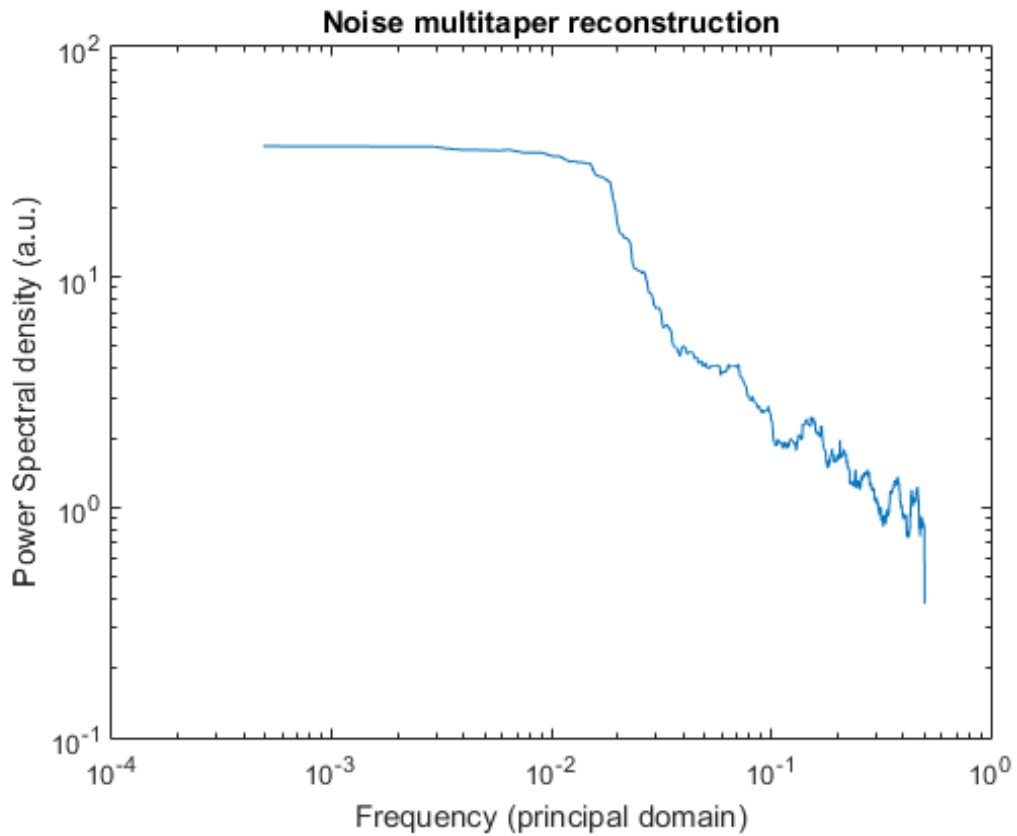
3.5.1 Measurement of Native Noise

Measuring and analysing the intrinsic noise in the VSG - qubit closed feedback loop provides two advantages. The information gained will not only help us justify which choices should be made about the noise strength and but will also give us an effective insight into the type of noise PSD which this system and similar setups will be experiencing. If the ultimate goal is to stabilise a system, it is imperative that a good understanding of the intrinsic noise PSD is obtained.

If we consider the spectral reconstruction of the native noise shown in figure 3.4b, we can see that it fits not white noise but rather a pink or $\frac{1}{\omega}$ noise. The other prominant feature is the flattening of the spectrum at lower frequencies. It is possible that the noise in the system is a combination of pink noise with a 'white top' *i.e.* a flat PSD at lower frequencies. Another possibility is that the experimentation was not done on enough measurements (1024 measurements) to effectively reconstruct the PSD. There is some evidence to suggest a reconstruction on longer experiments (> 16000 measurements) shows a more purely $\frac{1}{\omega}$ pink noise PSD [42, 41]. Regardless, this spectral construction instigated interest into the pink noise regime as that was previously considered unimportant. The trace shown in figure 3.4a is one of several
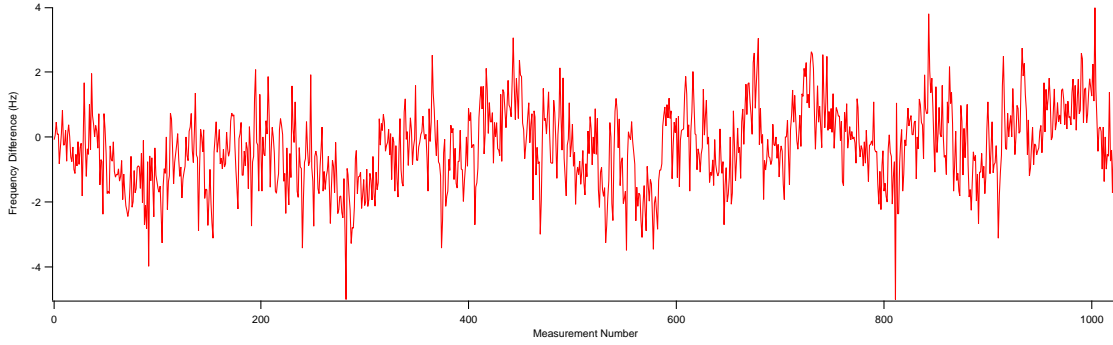
(a) 1024 measurements of native noise

(b) The spectral reconstruction of native noise PSD

**Figure 3.4:** After a long (approximately 1000 measurements) measurement recording (a) was taken with no deadtime or engineered noise, it was possible to analyse the small sample of intrinsic noise and take a Fourier transform after some signal processing to produce a reconstructed PSD of the noise in the VSG - qubit system (b). Note that the intrinsic noise fluctuates approximately ± 3 Hz

41

measurements taken and it was found that the calculated variance of the traces were independent of the timescale of the ramsey time as expected for pink noise [39].

3.5.2 Measurement of Engineered Noise in Time Domain
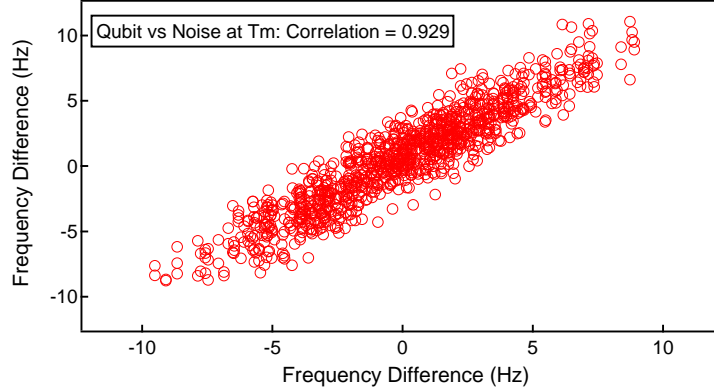
(a) Correlation plot of Qubit vs noise at time of measurement
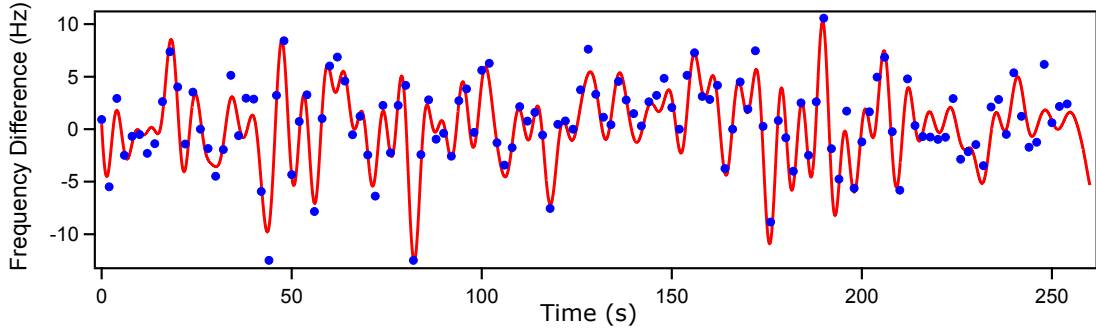
(b) Time domain pseudowhite noise trace with measurement

Figure 3.5: Results of measurement experiment show high fidelity quantum measurements in the presence of psuedowhite noise. The correlation plot (a) shows a high degree of association between the applied noise and the measured noise. The time domain plot (b) shows the measurements taken in real time along the application of noise. This experiment was performed with a 1% duty cycle on 20ms measurement times. The noise PSD parameters were the standard ones mentioned in section 3.4.2: $\omega_{start} = 0.001$ Hz, $\omega_{spacing} = 0.001$ Hz, $\omega_{stop} = 0.5$ Hz, PSD power $= 0$ and Noise Strength $= 0.85$.

It was important for the experimental platform to be able to take accurate measurements of time domain noise trace with any sensible set of measurement and noise parameters. In order to effectively visualise the accuracy of the quantum

measurements over time, experiments such as the one shown in figure 3.5 were performed and analysed. These experiments focused on taking measurements of approximately 20ms with a 1% duty cycle. Both flicker noise and pseudowhite noise were measured. Used as a metric for the fidelity of the measurement experiment was the correlation between the measurement and the noise at the time of measurement. Considering the result in Figure 3.5a, it can be seen that the measurement is highly correlated with the noise applied at the time of measurement (Correlation = 0.929), which suggest the system is effectively applying the noise and measuring a similar value using the double Ramsey experiment offset calculation method.

3.6 Traditional Measurement Feedback

The simpliest form of measurement based feedback describes the application of measurement information to a system for the purpose of maximising some measure of performance of minimising a certain cost function. For 'closed-loop' control, the system must either estimate or use measurements to gain information about the system to then provide the best dynamic action to optimise for some criteria. This usually takes the form of an output signal to the actuators with most effect said criteria. In the case of our qubit locked local oscillator feedback, the frequency of the output microwave field is the inherent or engineering noise source, the measured qubit frequency difference is the attempt to gain information about the system and the output frequency from the PC to the microwave VSG is the signal to the actuators.

Traditional techniques of locking a oscillator to a set frequency or phase involve the frequency deviation measurement to immediately used to correct the LO frequency, producing the more stable 'locked local oscillator'. It is also common to see deadtime between the measurement and correction due to electronic, experimental or mechanical necessities in the setup. [42] This traditional feedback approach is extremely sensitive to the addition of deadtime as any time between measurement and correction is accumulating further frequency or phase difference and hence
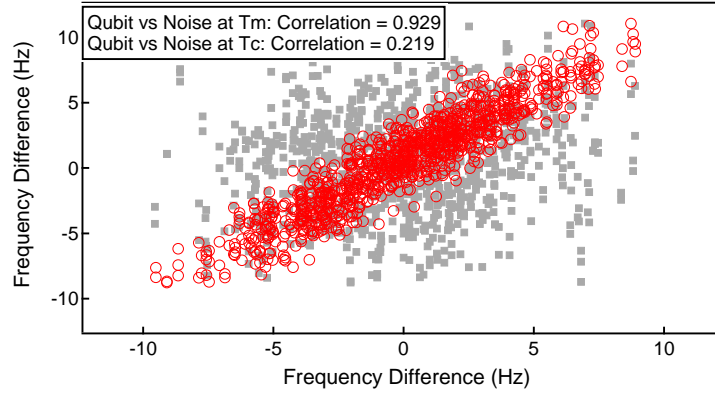
Figure 3.6: This correlation plot illustrates how information about the quantum state is lost over any given deadtime in the measurement process. The measurement correlation shown in 3.5a of 0.929 is all but lost over a 1% duty cycle. This gives a metric of the performance of the traditional feedback process as the only information of the state it can extract is from the previous measurement which is uncorrelated to the time of correciton.

producing an inaccurate feedback result. The effectiveness of the traditional feedback can be calculated by considering the correlation of the frequency noise at time of correction to the frequency at measurement as this will aptly show this accumulated frequency difference in the deadtime. This can be seen by Figure 3.6 as significantly uncorrelated. This confirms suspicions that, if the noise is fast changing with respect to this dead time, the previous measurement will lose value as a correctional point for feedback.

Chapter 4

Feedback beyond Quasistatic Limit

As seen in the previous chapters, using traditional feedback methods alone, it is impossible to extract information from the feedback system if the noise is fast changing in the deadtime. The transfer function approach is powerful because it may be employed to craft new measurement techniques based of previous noise trajectories. It has been postulated that these methods would provide an alternative to traditional feedback for state estimation and quantum control stability that could possibly provide accurate prediction even in regimes were the noise is fast compared to the deadtime. Classical control theory suggests many approaches such as linear regression and Kalman filtering. However, many of those techniques are difficult to implement in the quantum regime due to the characteristics discussed in section 1.2.

At the frontier of this research is the discussion of which algorithms will give the best results over certain noise power spectral densities and spurring conditions [42]. It has been suggested that an approach using a linear combination of measurements rather than just the information extracted from the last measurement could produce better results. The key insight is that the dominant noise processes in typical local oscillators are non-Markovian due to the low frequency bias in the PSD. This implys that there are temporal correlations in $y(t)$ that may be exploited to improve the feedback state estimation and stabilisation.

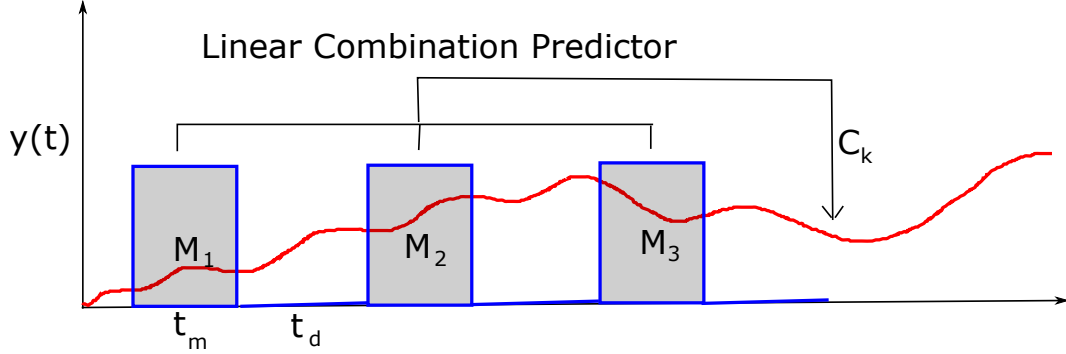## 4.1 Prediction Calculated from Linear Combinations of Measurements

Figure 4.1: Time-domain protocol schematic for calculating linear predictor. Three measurements of t_m measurement time seperated by t_d deadtime are combine to calculate prediction of state in future (C_k).

This linear combination would be combined with a set of weighting coefficients to produce a 'prediction' of the frequency noise at some time in the future (correction time, t_c). Therefore the prediction of the state at the correction time $(y(t_c))$ could be calculated by

$$y(t_c) = c_k.M_k \tag{4.1}$$

where c_k is the vector of weighting coefficients and M_k is the set of previous measurements. Calculating state prediction this way has commonly been referred to as *hybrid feedforward*, *predictive feedforward* or *covariance based prediction*. As we investigate this possibility, we must consider such questions as the number of previous measurements and the applications of calculated prediction. For example, if for n combined measurements, the prediction is applied after each nth measurement the weighting coefficient would be different if the correction was applied every cycle. These two methods are called non-overlapped and overlapped respectively.

In the coming sections of this chapter, the most fundamental question is attempted to be answered and experimentally implemented. This question is how should the

values of the coefficients be calculated to give the most accurate prediction of the noise at t_c in the future.

4.2 Calculating Coefficients from a Covariance Matrix

Following on from previous work done by Biercuk et al. [42], it can be shown that the weighting coefficients can be calculated from knowledge about the correlations between the noise power spectral density $(S(\omega))$ and the set of n previous measurements. Assuming that the LO noise is Gaussian and the linear least minimum mean squares estimator is optimal, a $n \times n$ square past observable measurement covariance matrix can be defined as follows;

$$\sigma(M_k) = \boldsymbol{V} = \begin{bmatrix} \sigma(M_{1,1}) & \sigma(M_{1,2}) & \cdots & \sigma(M_{1,n}) \\ \sigma(M_{2,1}) & \sigma(M_{2,2}) & \cdots & \sigma(M_{2,n}) \\ \vdots & \vdots & \ddots & \vdots \\ \sigma(M_{n,1}) & \sigma(M_{n,2}) & \cdots & \sigma(M_{n,n}) \end{bmatrix} \tag{4.2}$$

Combining this with the covariance vector of each past measurement observable with the future observable, F defined as

$$\sigma(M_k, F) = \boldsymbol{E} = \begin{bmatrix} \sigma(M_1, F) \\ \sigma(M_2, F) \\ \vdots \\ \sigma(M_n, F) \end{bmatrix} \tag{4.3}$$

the covariance matrix is extended to the complete covariance matrix

$$\sigma(M_k, y(t_c)) = \begin{bmatrix} \boldsymbol{V} & \boldsymbol{E}) \\ \boldsymbol{E^T} & \langle y(t_c)^2 \rangle \end{bmatrix} \tag{4.4}$$

47

The purpose of extending the covariance matrix to include F is to express the correlations between the noise at the time of correction $(y(t_c)$ and measurements preceding using the same transfer function formalisation that describes the correlations amongst the measurements themselves. It can be shown that the covariance is the scalar product of c_k and $\mathbf{E}$ [40] which means the covariance is maximised for $c_k \propto \boldsymbol{E}$. The true variance of the predictor is assumed to be equal to the instantaneous variance of the noise at the time of correction so the closed form expression for the weighting coefficients can be derived as:

$$c_k = \boldsymbol{E}\sqrt{\frac{\langle y(t_c)^2 \rangle}{\boldsymbol{E^T V E}}} \tag{4.5}$$

In experimental simulation, this requires calculation of $\langle y(t_c)^2 \rangle$ which is possible given the noise PSD (Sω)). In order to effectively calculate these coefficients and metrics of performance of this predictive feedforward method, a numerical model of an LO undergoing the measurement and correction protocol was written in *MATLAB 2015a*. The simulation code takes an arbitrary piecewise noise PSD function, the number of measurement bins, duty cycle and timing values to evaluate the covariance matrix at the time of correction and apply correction coefficients to noise at that time. If this is run repeatedly, it is possible to calculate sample variance of each prediction compared to traditional feedback techniques.

This predictive method proposed makes explicit use of S(ω) to optimise the measurement protocol and completely collapses without that information. The covariance predictive method is expected to perform better than traditional feedback as it able to combine many measurements over different time periods on the noise trace and hence sample larger portions of the noise spectrum. As knowledge of the noise power spectral density might not always be available, a method which requires no knowledge of S(ω) was considered.

4.3 Calculating Coefficients from Brute Force Search

In order to calculate the weighting coefficients over a noise trace with only experimental data, a series of MATLAB scripts were written in order to search the $(n+1)$-dimensional space for the optimal coefficients for n measurements. The cost function for such a optimisation is as follows;

$$C(\boldsymbol{c_k}) = corr(y_p(t_c), y(t_c)) = corr(\boldsymbol{c_k}.\boldsymbol{M_k}, y(t_c)) \tag{4.6}$$

where $\boldsymbol{c_k}$ is a n-dimensional vector of the weighting coefficients. The first design decision in this script was the extend the space to include a constant shown in equation 4.7.

$$y_p(t_c) = c_1 M_1 + c_2 M_2 + \cdots + c_n M_n + c_{n+1} \tag{4.7}$$

This constant (c_{n+1}) was added to cancel out any inherent offset that existed in the noise trace. Using this formulation, it was possible to search the common coefficient space ($-1.5 < c_k < 2.5$) for each of the unknowns in an attempt to maximise accuracy. A 'comb' of potential coefficients were constructed in a similar fashion to the method used in noise engineering. Between the common values of coefficients, a minimum step size (c_{step}) was selected to test values. Obviously it is possible to select an infinitely small step size for maximum resolution. However due to the nature of the program, the step size was proportional to the computation time. By considering the MATLAB operation timings, it was found that;

$$T_{comp} \propto \left(\frac{c_{stop} - c_{start}}{c_{step}} \right)^n \tag{4.8}$$

so it a optimal value for c_{step} had to be chosen in order to maximise resolution in resonable computational times. It was found that past approximately 10^{-4} the increased accuracy of c_{step} did not give any improvements in the cost function so no

further resolution was considered necessary. At this step size and for 3 measurements the computational time was approximately 5 hours.

A second metric of accuracy used was the root mean square error (RMSE) of the difference between the prediction and the noise at the time of correction. This second cost function was calculated in an attempt to contrast different visualisations of the results. Both metrics produced very similar results when used to maximise for coefficient inputs. In order to optimise the coefficients, a sample of uncorrected data (a generated noisetrace and measurements taken at regular intervals) was taken experimentally and then a subsection of this data was taken and labeled 'training data'. Over this data set, predictions were calculated for specific points, $y_p(t_c)$ in the future in an overlapping configuration.
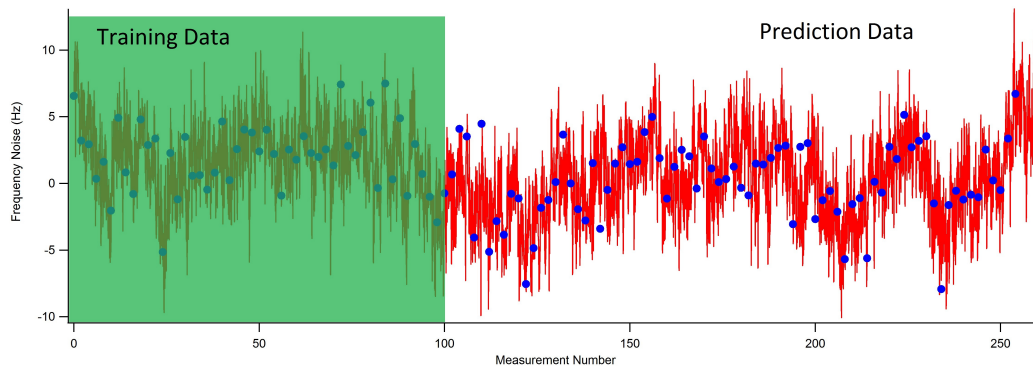

Figure 4.2: Example of methodology used on uncorrected data to split in 'training data' (approximately the first 100 measurments) and 'prediction data' in an attempt to optimise the coefficients over the former section and test them over the latter section.

Once coefficients have been found to maximise correlation (Γ) for the first set of data (training data), those coefficients were used blindly to calculate predictions on the remaining prediction data. It is then possible to analyse the accuracy of the prediction data using a similar correlation method shown in equation **??**

It should be noted that this method of optimisation was chosen due to its simplicity and ease of implementation swiftly into the experimental setup. A typical 'training'

	Covariance Matrix Method	Brute Force Method
c_1	0.6786	-0.2541
c_2	0.1235	0.2256
c_3	0.8801	0.8824
c_4	-	0.0015

Table 4.1: Comparison of Coefficients Calculated by Covariance and Brute Force Methods. The coefficients are very similar be diverge slightly at the first coefficient. These coefficients were calculated on a psuedowhite noise trace with 3 measurement bins. The brute force method also includes a constant (c_4

process was extremely computationally intensive and would take anywhere between 20 minutes and 7 hours depending on the degree of accuracy required in the coefficients.

Comparison of Coefficients Calculated by Covariance and Brute Force Techniques

A major benefit of calculating weighting coefficients in two separate ways was that it allowed us to compare and contrast the results of both. Table 4.1 shows the results of an example calculation on pseudowhite noise with a 50ms measurement time and 10% duty cycle. It can be seen that both methods somewhat agree with only a slight deviation in the first coefficient. This deviation was increased with the addition of the constant in the brute force method so it is possible it is conceived by the prediciton offset. This would have a greater effect on the measurements and hence the coefficients at a greater time from the time of correction.

4.4 Experimental Feedback Results

In order to assess whether linear combinations of measurements will produce improved performance for oscillator stability and state estimation experimental results must be presented.

4.4.1 Oscillator Stability

As mentioned previously, the common metric used for oscillator stability is *variance* and it is measured experimentally in order to show that a linear combination of measurements performs better as a passive frequency standard feedback technique. The experimental procedure to measure oscillator stability involves real time correction of the local oscillator over a series of measurements. The state of the qubit was measured at each point given a certain deadtime and corrected by changing the input to the local oscillator to account for the noise measurement made in the previous bins. In post processing, it is then possible to calculate the variance of each qubit measurement against the applied noise on the local oscillator. This is practically comparing the performance of the oscillator stability against the 'real' noise trace.
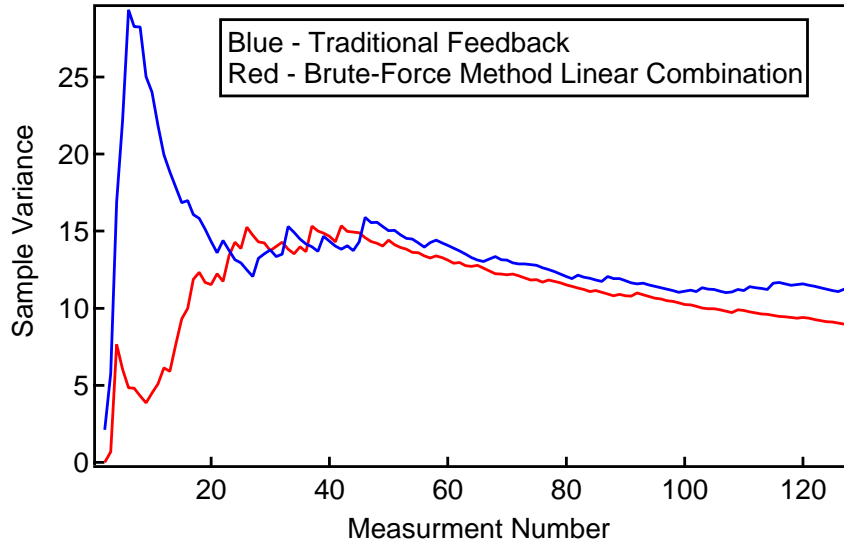

Figure 4.3: Experimental demonstration of predictive feedforeword. This experiment was performed an engineered psuedowhite noise with an upper cutoff $\omega_{stop} = 0.5$ Hz and lower cutoff $\omega_{start} = 1$ mHz. The sample variance is calculated for all of the previous measurements and the predictive method (red) is shown to result in a lower sample variance over only 128 measurements. The duty cycle of this measurement scheme was 1% with 20ms measurements with active real time correction.

This real time correction and variance calculation is performed for traditional feedback and predictive feedforward methods to directly compare the variance over time. Figure 4.3 shows the success of linearly combining measurements using the brute-force calculation method. The initial instability in the figure (measurements number < 45) is due to the lack of measurements taken. Over time the variance flattens and slowly reduces as the feedback techniques stabilise the local oscillator. This experimental demonstration shows the predictive feedforward reducing the variance over 128 measurements by a factor of approximately 0.2.
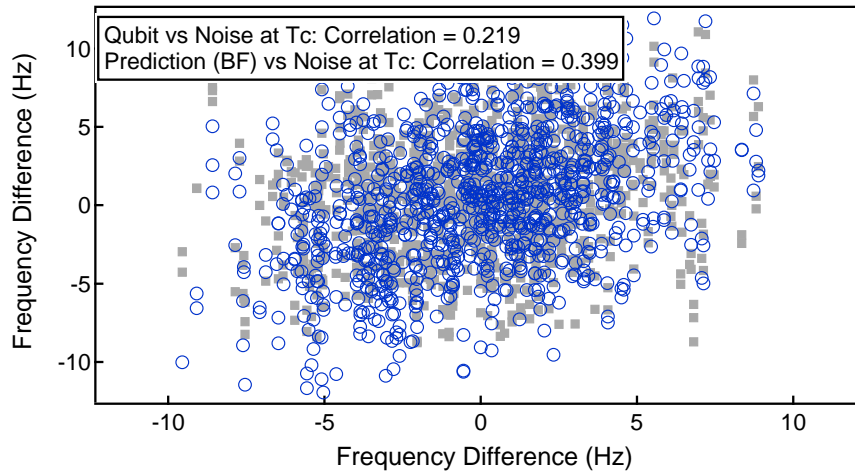
4.4.2 State Estimation

In order to continue research on the predictive feedforward techniques and the complete the performance picture, the question of accuracy was raised. Rather than considering the sample variance corrected over time, a simpler experiment was run concerning the ability to predict a noise state given n previous measurements. To perform this experimentally a measurement set similar to the one shown in Figure 3.5b was taken and analysed offline. Each measurement was collected into groups of n measurements (commonly three bins) and used to predict the noise at some point in the future (t_c). These predictions were calculated using equation 4.1 where the coefficients were calculated from both feedforward methods. Similar to the analysis of traditional feedback and the free evolution of the noise over some deadtime, the correlation between the prediction and the noise at the time of correction are shown in Figure 4.4.

The results shows a reduction in the uncorrelated spread of noise at t_c against the previous measurement. This is shown visually and with statistical analysis. As these methods which used combinations of measurements, extra more information could be extracted from the noise spectral density which results in a more accurate prediction of the noise than using just one previous measurement. The coefficient calculated by brute force have performed slightly better in this regime.
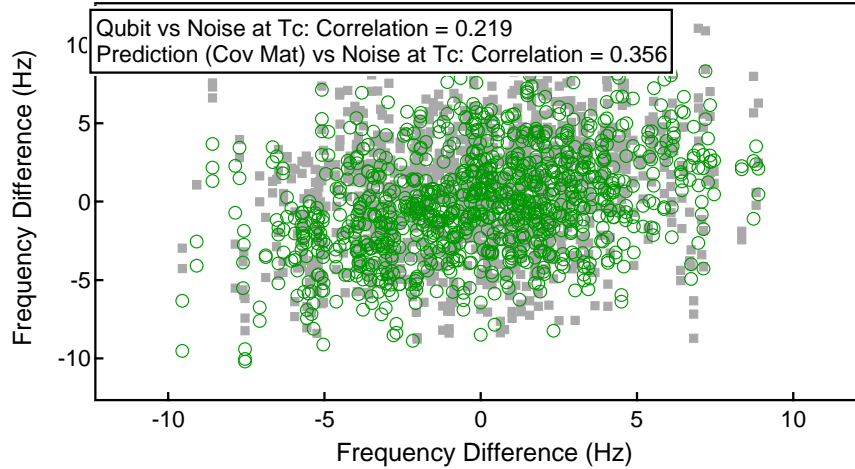
(a) Covariance Matrix Method

(b) Brute Force Method

Figure 4.4: Assessment of state estimation accuracy for both the covariance method (a) and brute force (b) method of calculating coefficients. In both plots the y axis is the predicted qubit-LO frequency difference and the x-axis the applied frequency difference. The reduction in spread shows an increase in accuracy over the free evolution (traditional feedback) shown in gray. Both plots were constructed in post processing on experimental data taken with the Ytterbium trap. The parameters of the experiment were the same as listed in Figure 4.3 however the active stabilisation was turned off in data collection and prediction applied later.

Another area where predictive feedforward shows significant success over traditional feedback is with predictions at times greater than one cycle time. A similiar analysis was performed again on a data set but rather with coefficients that predict
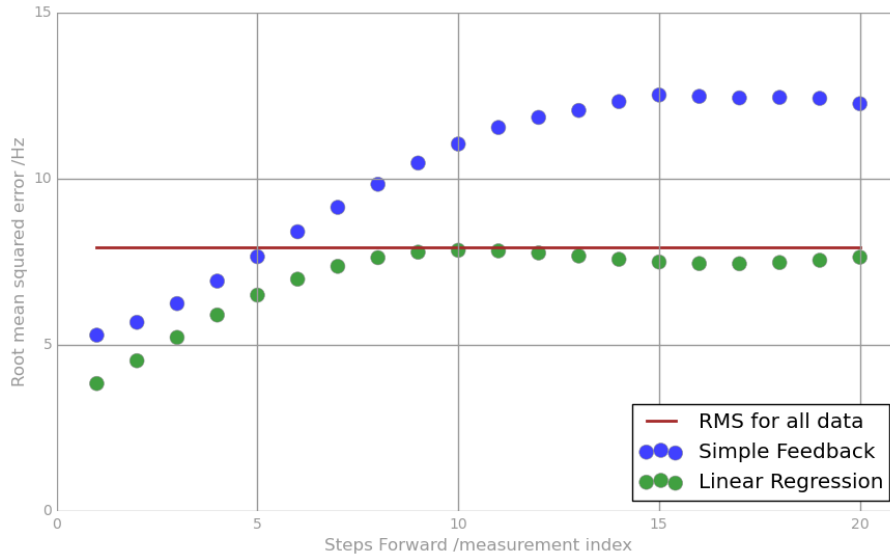
Figure 4.5: Analysis of prediction accuracy at times greater in the future than one cycle time. Each cycle time is referred to as a 'step' on the x axis.The RMSE is calculated for a set of differences between prediction and applied noise at each step. As the RMSE is a metric of the accuracy, the reduced error in the predictive feedforward data set (green shows a better performance at greater times in the future. The RMS for all the data is also plotted to give a reference of the magnitude of noise in the data. All data was taken in the same way as the previously mentioned state estimation.

at integer multiples of the cycle time into the future. The root mean square error of each of these sets were than calculated to measure the performance over time. Figure 4.5 shows that at greater times in the future, the RMSE of the measurement to the prediction and hence the accuracy remains lower for the predictive feedforward than the traditional feedback.

Chapter 5

Conclusion

This thesis presents the complete description and analysis for feedback techniques for stablising a local oscillator using a qubit reference. Specifically, the ability of predictive feedforward techniques are compared against traditional feedback. Chapter 1 clearly defines the motivation behind working on quantum control techniques and the problems encountered in the field. Chapter 2 looks at the experimental platform; the Ytterbium ion trap and gives both the theoretical description of the underlying physics and engineerings as well as the specifics of the constructed and run experimental setup. Chapter 3 derives many of the noise engineering methods and in later sections introduces the concept of reliable measurement based feedback. Chapter 4 presents the derivation of methods to use linear combinations of methods to calculation noise states and analyses the results of performed experiments on these techniques.

Ultimately, this thesis presents experimental contributions to the field of quantum precision control. Improved techniques for measuring qubit frequency and oscillator frequency feedback techniques have been demonstrated and analysed in a way that nobody has before experimentally. We have built a good case to argue that linear combinations of measurements give greater stability (lower sample variance of qubit to oscillator) than traditional one measurement feedback in a locked oscillator scenario.

This thesis has also shown that linear combinations create more accurate state predictions than the previous measure information would give.

Along with this, the simulation scripts written in MATLAB have provided excellent metrics on the degree of improvement one technique should give over another in specific noise power regimes. These metrics will be the benchmark of understanding and performance for further experimentation and implementations of this type.

By studying multiple methods of producing weighting coefficients for linear combination prediction has given us theoretical insight the value of understanding the power spectral density of the systems noise. Calculating coefficients by covariance between he measurements and a future state known from the PSD and searching the variable space for the coefficients resulted in very similar degrees of accuracy in state estimation and oscillator stability. This provides flexibility for implementation in real frequency standard systems.

5.1   Direction of Future Research

As with any experimental engineering, this thesis creates more questions than it answers. The experimental results shown in chapter 4 is the first complete demonstration of improved oscillator performance using combinations of measurements. This result provides an extremely sound starting point for further investigation. Moving forward, exploration of the performance of the feedforward technique over a greater range of experimental parameters including power spectra, measurement and duty cycles. This exhaustive parameter survey would expand the body of knowledge on this technique and allow engineers to better assess it applicability to real experiment and industrial passive frequency standards. Not only has the technique got foreseeable benefits in the field of frequency standards but with further understanding may lead to much broader uses in quantum information theory and quantum state estimation.

The simulation and analysis code provide a solid foundation of understanding regarding the performance metrics, however multiple extensions could be made to

further understanding. A major addition to the brute-force calculation code would be to map the cost function landscape to better understand the local maxima and minima. The ultimate motivation of mapping the landscape experimentally is valid the theoretical understanding of this technique. As well as this, the experimentation presented in this thesis focused almost solely on three bin measurements as an arbitrary starting place. Extension of both the MATLAB code and understanding of how greater sets of measurements effect the prediction ability is extremely important.

Bibliography

[1] H. Ball and M. J. Biercuk. Walsh-synthesized noise filters for quantum logic. *EPJ Quantum Technology*, 2, 2015. 30

[2] J. A. Barnes, A. R. Chi, L. S. Cutler, D. J. Healey, D. B. Leeson, T. E. McGunigal, J. A. Mullen, W. L. Smith, R. L. Sydnor, R. F. C. Vessot, and G. M. R. Winkler. Characterization of frequency stability. *IEEE Trans. Instr. and Meas.*, 20, 1971. 8

[3] J. Bergou and M. Orszag. Dynamically correlated spontaneous-emission laser: theory and comparison with experiment. *Journal of the Optical Society of America B*, 5, 1988. 28

[4] M. J. Biercuk, A. C. Doherty, and H. Uys. Dynamical decoupling sequence construction as a filter-design problem. Archived, 2011. 7

[5] J. M. Blackledge. *Digital Signal Processing: Mathematical and Computational Methods, Software Development and Applications*. Horwood Publishing, 2003. 38

[6] R. Blatt and D. J. Wineland. Entangled states of trapped atomic ions. *Nature*, 453, 2008. 12

[7] B. H. Bransden. *Physics of Atoms and Molecules*. Pearson Education, 2003. 31

[8] L. S. Brown and G. Gabrielse. Geonium theory: Physics of a single electron or ion in a penning trap. *Rev. Mod. Phys.*, 58:233, 1986. 12

[9] O. Crisafulli, N. Tezak, D. B. S Soh, M. A. Armen, and H. Mabuchi. Squeezed light in an optical parametric oscillator network with coherent feedback quantum control. Archived, 2014. 8

[10] L. S. Cutler and C. L. Searle. Some aspects of the theory and measurement of frequency fluctuations in frequency standards. *Proceedings of the IEEE*, 54, 1966. 8

[11] S. Datta and B Das. Electronic analog of the electro-optic modulator. *Appl. Phys. Lett.*, 56, 1990. 22

[12] P. TH. Fisk. Trapped-ion and trapped-atom microwave frequency standards. *Reports on Progress in Physics*, 60, 1997. 12

[13] P. TH. Fisk, M. J. Sellars, M. A. Lawn, and C. Coles. Accurate measurement of the 12.6 ghz clock transition in trapped 171yb+ ions. *IEEE Transactions on Ultrasonics, Ferroelectrics and Frequency Control*, 44, 1995. 17

[14] C. J. Foot. *Atomic Physics*. Oxford University Press, 2005. 6

[15] J. M. Geremia. An introduction to control theory from classical to quantum applications; control theory course notes, 2003. 1

[16] T. J. Green, J. Sastrawan, H. Uys, and M. J. Biercuk. Arbitrary quantum control of qubits in the presence of universal noise. *New Journal of Physics*, 15, 2013. 6

[17] D. J. Griffiths. *Introduction to Electrodynamics*. Prentice Hall, 1999. 12

[18] D. J. Griffiths. *Introduction to Quantum Mechanics*. Pearson Education, 2005. 3

[19] D. L. Hayes. *Remote and Local Entanglement of Ions using Photons and Phonons*. PhD thesis, University of Maryland, 2009. 17, 18

[20] W. M. Itano, J. C Bergquist, J.J Bollinger, and D. J. Wineland. Cooling methods in ion traps. *Physica Scripta*, 106, 1995. 19

[21] M. C. Jarratt. Uv light sources for 171yb+ ion trap experiments. Master's thesis, University of Sydney, 2013. 22, 23

[22] M. W. Lee, M. C. Jarratt, C. Marciniak, and M. J. Biercuk. Frequency stabilization of a 369 nm diode laser by nonlinear spectroscopy of ytterbium ions in a discharge. *Optics Express*, 22, 2014. 23

[23] L. L. Lewis. An introduction to frequency standards. *Proceedings of the IEEE*, 79, 1991. 8

[24] J. McLoughlin. *Development and Implementation of an Yb+ Ion Trap experiment towards coherent manipulation and entanglement.* PhD thesis, University of Sussex, 2011. 17

[25] H. J. Metcalf and P. van der Straten. *Laser Cooling and Trapping.* Springer-Verlag New York, Inc, 1999. 19

[26] G. J. Milburn. *Schrödinger's Machines.* W H Freeman and Company, 1997. 1

[27] C. D. Motchenbacher and J. A. Connelly. *Low-noise electronic system design.* Wiley Interscience, 1993. 36

[28] W. Neuhauser, M. Hohenstatt, P. Toschek, and H. Dehmelt. Optical-sideband cooling of visible atom cloud confined in parabolic well. *Phys. Rev. Lett.*, 41:233, 1978. 19

[29] M. A. Nielson and I. L. Chuang. *Quantum computation and Quantum Information.* Cambridge University Press, 2010. 2

[30] M. P. Norton and D. G. Karczub. *Fundamentals of Noise and Vibration Analysis for Engineers.* Cambridge University, 2003. 34

[31] K. Odaka and S. Ueda. Dependence of outgassing rate on surface oxide layer thickness in type 304 stainless steel before and after surface oxidation in air. *Vacuum*, 47, 1996. 26

[32] S. M. Olmschenk, K. C. Younge, D. L. Moehring, D. N. Matsukevich, P. P. Maunz, and C. Monroe. Manipulation and detection of a trapped yb+ hypefine qubit. *Phys. Rev. A*, 76, 2007. 16

[33] S. M. Olschenk. *Quantum Teleportation Between Distant Matter Qubits*. PhD thesis, University of Michigan, 2009. 11, 14, 17, 25

[34] W. Paul. Electromagnetic traps for charged and neutral particles. *Rev. Mod. Phys.*, 62:531, 1990. 12

[35] J. D. Prestage, G. J. Dick, and L. Maleki. Linear ion trap based atomic frequency standard. *Proceedings of the 44th Annual Symposium on Frequency Control*, 1990. 13

[36] K. Pyka. *High-precision ion trap for spectorscop of Coulomb crystals*. PhD thesis, University of Hannover, 2013. 18

[37] N. F. Ramsey. The method of successive oscillatory fields. *Physics Today*, 66, 2013. 31

[38] T. Rosenband, D.B. Hume, P. O. Schmidt, C. W. Chou, A. Brusch, L. Lorini, W. H. Oskay, R. E. Drullinger, T. M. Fortier, J.E. Stalnaker, S. A. Diddams, W. C. Swann, N. R. Newbury, W. M. Itano, J.C. Bergquist, and D. J. Wineland. Frequency ratio of al$^+$ and hg$^+$ single-ion optical clocks; metrology at the 17th decimal place. *Science*, 319, 2008. 12, 31

[39] J. Rutman. Characterization of phase and frequency instabilities in precision frequency sources: Fifteen years of progress. *Proceedings of the IEEE*, 66, 1978. 35, 42

[40] J. Sastrawan. Predictive feedforward for passive frequency standards, 2013. 6, 48

[41] J. Sastrawan. Novel precision control techniques in a trapped yb+ ion implementation. Master's thesis, University of Sydney, 2015. 11, 19, 23, 28, 29, 33, 40

[42] J. Sastrawan, C. Jones, I. Akhalwaya, H. Uys, and M. J. Biercuk. Improving frequency standard performance by optimized measurement feedback. Archived, 2014. 2, 31, 40, 43, 45, 47

[43] T. Schulte-Herbruggen, A. Sporl, N. Khaneja, and S. J. Glaser. Optimal control-based efficient synthesis of building blocks of quantum algorithms: A perspective from network complexity towards time complexity. *Phys. Rev.*, 72, 2006. 2

[44] S. A. Schulz, U. Poschinger, F. Ziesel, and F. Schmidt-Kaler. Sideband cooling and coherent dynamics in a microchip multi-segmented ion trap. *New J. Phys.*, 73, 2008. 19

[45] M. D. Shulman, S. P. Harvey, J. M. Nichol, S. D. Bartlett, A. C. Doherty, V. Umansky, and A. Yacoby. Suppressing qubit dephasing using real-time hamiltonian estimation. *Nature Communications*, 5, 2014. 2

[46] S. Skogestad and I. Postlethwaite. *Multivariable Feedback Control*. Wiley and Sons, 1996. 1

[47] A. Soare. Agile 12.6 ghz microwave system for the robust quantum control of trapped 171yb+ ions. Master's thesis, University of Sydney, 2012. 29

[48] A. Soare, H. Ball, D. Hayes, J. Sastrawan, M. C. Jarratt, J. J. Loughlin, X. Zhen, T. J. Green, and M. J. Biercuk. Experimental noise filtering by quantum control. *Nature Physics*, 10, 2014. 7

[49] A. Soare, H. Ball, D. Hayes, J. Sastrawan, M. C. Jarratt, X. Zhen, H. Uys, and M. J. Biercuk. Experimental bath engineering for quantitative studies of quantum control. *Phys. Rev. A*, 89, 2014. 37

[50] R.F. Stengel. *Optimal Control and Estimation.* Dover Publications, 1996. 1

[51] G. S. Uhrig. Keeping a quantum bit alive by optimized -pulse sequences. *Phys. Rev. Lett.*, 98, 2007. 30

[52] L. M. K. Vandersypen and I. L. Chuang. Nmr techniques for quantum control and computation. *Rev. of Mod. Phys.*, 76, 2005. 7

[53] D. Vion, A. Aassime, A. Cottet, P. Joyez, H. Pothier, C. Urbina, D. Esteve, and M. H. Devoret. Rabi oscillations, ramsey fringes and spin echoes in an electrical circuit. *Fortschr Phys.*, 51, 2003. 32

[54] N. Weiner. Generalised harmonic analysis. *Acta Mathematica*, 55, 1930. 35

[55] G. Werth. *Lecture Notes in Physics.* Springer Berlin Heidelberg, 2008. 13

[56] D.J. Wineland, R. E. Drullinger, and F. L. Walls. Radiation pressure cooling of bound resonant absorbers. *Phys. Rev. Lett.*, 40:1639, 1978. 19

Appendix

Appendix A

MATLAB Code

```matlab
%DEFINE ANALYSIS PARAMETERS

deadtime = 1980;
ramsey = 20;
cycle = deadtime + ramsey;
measnum = 1024;
noise = Sept1519noisetrace;
qubit = Sept1519qubit;
coeff = [0.7,-0.9,0.85];
AhffHighest = 0;
coeffHigh = [0,0,0];
i=1:measnum;
percent=0;

%CALCULATE VECTOR INDEXES
k1 = 401:400:409601;
noiseTc = noise(k1,:);

k2 = 3:400:409203;
noiseTm = noise(k2,:);
```

```matlab
plot(noiseTc(:,2),qubit(:,2),'*');


predict = NaN(measnum,2);



for d = -1:0.01:1
    for a=-1:0.5:1.5
        for b=-1:0.5:1.5
            for c=-1:0.5:1.5

                coeffOp =[a,b,c];
                for j=1:measnum-2;
                  measure = [qubit(j,2); qubit(j+1,2); qubit(j+2,2)];
                  predictOp(:,1) = noiseTc(:,1);
                  predictOp(1:2,2) = NaN;
                  predictOp(j+2,2) =dot(coeffOp,measure);
                  predict(:,1) = noiseTc(:,1);
                  predict(1:2,2) = NaN;
                  predict(j+2,2) =dot(coeff,measure);
                end

                %hold on
                %plot(noiseTc(:,2),predict(:,2), 'r*');
                A_tfb = corr(noiseTc(3:measnum,2),qubit(3:measnum,2));
                A_hffOp = corr(noiseTc(3:measnum,2),predictOp(3:measnum,2));

              if A_hffOp > AhffHighest
                  AhffHighest = A_hffOp;
                  coeffHighest = coeffOp;
              end
            end
        end
    end
```

```
        percent = (percent+1)
    end
end
A_hff = corr(noiseTc(3:measnum,2),predict(3:measnum,2));
```